

Highlights (for review)

# Highlights

- Multipeak analysis provides greater insight into phase behavior than laurdan GP.
- Multipeak analysis of laurdan spectra agrees with phase behavior of giant vesicles.
- Hybrid lipid/polymer vesicles display phase separation at high cholesterol levels.
- Multipeak analysis may reveal phase separation mechanisms in hybrid vesicles.

Characterization of phase separation phenomena in hybrid lipid/block copolymer/cholesterol bilayers using laurdan fluorescence with log-normal multipeak analysis

Naomi Hamada <sup>a</sup> and Marjorie L. Longo <sup>\*a</sup>

<sup>a</sup> Department of Chemical Engineering, University of California Davis, Davis, California 95616, United States

\*Corresponding authors: e-mail address: mllongo@ucdavis.edu

# **Abstract**

Phase separation phenomena in hybrid lipid/block copolymer/cholesterol bilayers combining polybutadiene-block-polyethylene oxide (PBdPEO), egg sphingomyelin (egg SM), and cholesterol were studied with fluorescence spectroscopy and microscopy for comparison to lipid bilayers composed of palmitoyl oleoyl phosphatidylcholine (POPC), egg SM, and cholesterol. Laurdan emission spectra were decomposed into three lognormal curves. The temperature dependence of the ratios of the areas of the middle and lowest energy peaks revealed temperature break-point (T<sub>break</sub>) values that were in better agreement, compared to generalized polarization inflection temperatures, with phase transition temperatures in giant unilamellar vesicles (GUVs). Agreement between GUV and spectroscopy results was further improved for hybrid vesicles by using the ratio of the area of the middle peak to the sum of the areas all three peaks to find the T<sub>break</sub> values. For the hybrid vesicles, trends at T<sub>break</sub> are hypothesized to be correlated with the mechanisms by which the phase transition takes place, supported by the compositional range as well as the morphologies of domains observed in GUVs. Low miscibility of PBdPEO and egg SM is suggested by the finding of relatively high T<sub>break</sub> values at cholesterol contents greater than 30 mol%. Further, GUV phase behavior suggests stronger partitioning of cholesterol into PBdPEO than into POPC, and less miscibility of PBdPEO than POPC with egg SM. These results, summarized using a heat-map, contribute to the limited body of knowledge regarding the effect of cholesterol on hybrid membranes, with potential application toward the development of such materials for drug delivery or membrane protein reconstitution.

Keywords: hybrid vesicles; membrane phase behavior; liquid-ordered; copolymer; fluorescence spectroscopy; multipeak analysis

# 1. Introduction

Hybrid membranes combining lipids and amphiphilic block copolymers have been a recent area of scientific interest, especially because of their potential value toward biomedical applications. Both lipid membranes and block copolymer membranes individually offer unique advantages, motivating the study of hybrid membranes. While the biocompatibility of lipid membranes has facilitated their usage in the areas of liposomal drug delivery and membrane protein reconstitution, the wide range of chemical functionality and increased mechanical stability of block copolymer membranes are also desirable [1]. Such hybrid membranes are thus appealing because they combine the favorable properties of both lipid and block copolymer membranes. In comparison to lipid-only or polymer-only membranes, hybrid membranes have been demonstrated to extend the functional lifetime of an incorporated membrane protein [2] and to increase the yield of cell-free expression of a membrane protein [3]. Hybridization of polymer vesicles with lipids has also been demonstrated to increase the efficacy of targeted vesicle binding to tumors in mice [4].

To further inform the application of hybrid membranes, it is important to understand their phase behavior, as this may have implications toward their function. For example, in lipid vesicles the formation of domains enriched in a cationic lipid has been suggested to enhance intracellular delivery of macromolecules [5,6]. The phase behavior of lipid membranes has been studied extensively. It is well documented that in the presence of cholesterol, certain lipid mixtures can display solid/fluid or fluid/fluid phase separation depending upon the mixture composition [7–9]. Similarly, phase separation in hybrid membranes has been reported for a variety of compositions [1,10]. However, the effect of cholesterol on the phase behavior of block copolymer and hybrid membranes has been explored to only a limited extent [10,11]. There thus exists a need for continued investigation of the phase behavior of hybrid membranes.

Fluorescent probes, including diphenylhexatriene (DPH) [12] and laurdan [13], have been used to study the phase behavior of both lipid-only [12–15] and hybrid membranes [16,17]. For this work, laurdan was chosen due to its greater sensitivity to the phase behavior of hybrid dipalmitoylphosphatidylcholine (DPPC)/polybutadiene-block-polyethylene oxide (PBdPEO) vesicles which we demonstrated in recent work [16]. Laurdan displays a red shift in its emission spectrum as the polarity of its local environment increases [13]. This is directly related to the hydration of the membrane, which is in turn dependent on the extent of the ordering of the membrane. The relative membrane polarity indicated by laurdan is quantified by calculation of generalized polarization (GP) values. Trends in laurdan GP values thus provide information regarding the phase behavior of the membrane [13]. To gain further insight into the phase behavior of lipid membranes, decomposition of laurdan emission spectra into multiple peaks has been proposed as an additional tool [18–20]. For the case of cholesterol-containing lipid membranes in particular, multipeak analysis has been proposed to provide greater insight into phase behavior than calculation of GP values [18]. Because the emission wavelength of laurdan depends strongly

on the polarity of the membrane, trends observed in the relative areas of the peaks returned by such decomposition approaches have been reported to correspond with the phase behavior of the membrane [18,19].

Here, we apply multipeak analysis to laurdan emission spectra, taken at sequential temperatures, of 3-component vesicles composed of the block copolymer PBdPEO or the lipid palmitoyl oleoyl phosphatidylcholine (POPC), egg sphingomyelin (egg SM), and cholesterol. This technique has not been used with hybrid membranes before, to the best of our knowledge, but presents a means of studying their phase behavior in greater depth than possible with the more general information provided by trends in laurdan GP values. A PBdPEO block copolymer with an average molecular weight of 950 g/mol, expected to form a relatively fluid membrane at room temperature [21], was used. Vesicles combining either POPC (solid-fluid transition temperature of -2 °C) or PBdPEO (glass transition temperature of ~-22 °C) and egg SM (solid-fluid transition temperature of ~39 °C [7]) are first compared as POPC and PBdPEO are expected to be fluid and egg SM is expected to be solid at room temperature. Then, analysis of laurdan emission spectra for lipid-only vesicles containing POPC, egg SM, and cholesterol is presented for a limited range of compositions. Subsequently for a broad range of compositions, laurdan emission spectra for hybrid vesicles containing PBdPEO, egg SM, and cholesterol is presented. For both hybrid and lipid-only vesicles with cholesterol, the phase behavior indicated by multipeak analysis is found to be in better agreement with fluorescence microscopy results in giant unilamellar vesicles (GUVs) than that indicated by laurdan GP values. Similar to the phase behavior reported for lipid-only vesicles [7], both solid/fluid and fluid/fluid phase separation are observed for hybrid GUVs containing cholesterol. Overall, our results suggest stronger partitioning of cholesterol into the copolymer PBdPEO than into POPC, and less miscibility of PBdPEO with egg SM in comparison to POPC and egg SM.

#### 2. Materials and Methods

#### 2.1 Materials

Egg sphingomyelin (egg SM), palmitoyl oleoyl phosphatidylcholine (POPC), egg lissamine rhodamine B phosphatidylethanolamine (egg rhod PE), and cholesterol were purchased from Avanti Polar Lipids, Inc. The diblock copolymer poly(1,2-butadiene)-*block*-poly(ethylene oxide) (PBdPEO), with an average molecular weight of 950 g/mol, (P41807C-BdEO, Bd(600)-b-EO(350), PDI = 1.06) was purchased from Polymer Source, Inc. 6-dodecanoyl-2-dimethylaminonaphthalene (laurdan) was purchased from AdipoGen Life Sciences. Texas Red 1,2-dihexadecanoyl-sn-glycero-3-phosphoethanolamine (Texas Red DHPE) was purchased from Biotium. All water used for experiments was purified with a Barnstead Nanopure System (Barnstead Thermolyne) and had a resistivity  $\geq$ 17.8 M $\Omega$ ·cm.

### 2.2 Preparation of large unilamellar vesicles (LUVs)

Appropriate volumes of lipid, polymer, and cholesterol stock solutions in chloroform and laurdan stock solution in ethanol were combined in clean glass vials. A gentle stream of nitrogen was used to evaporate the solvent, leaving a uniform film. To remove any residual solvent, the vials were then kept under vacuum for 2-24 hours. The dried film was heated in a water bath of at least 50 °C and rehydrated with water to a final lipid/polymer concentration of 2 mM. This solution was then passed 11 times through a polycarbonate membrane with 0.1 μm pores using a mini extruder (Avanti).

# 2.3 Preparation of giant unilamellar vesicles (GUVs)

Appropriate volumes of lipid, polymer, and cholesterol stock solutions in chloroform were combined in a clean glass vial and further diluted with chloroform to vield a final lipid/polymer concentration of 0.5 mg/mL. 0.2 mol% of egg rhodamine PE was incorporated into lipid-only giant unilamellar vesicles (GUVs); the same concentration of Texas Red DHPE was used instead for hybrid GUVs. The mole percentage of the lower melting temperature component (POPC or PBdPEO) was reduced in compensation. GUVs were prepared in a custom built electroformation chamber consisting of parallel platinum electrodes in a polytetrafluoroethylene housing. 25 µL of the prepared stock solution was spread over each electrode with a gastight Hamilton glass syringe, and a gentle stream of nitrogen was used to dry the electrodes. The chamber was then placed under vacuum for 2-24 hours to remove any residual solvent. Immediately prior to vesicle formation, glass coverslips were fixed over the openings of the chamber with vacuum grease and the sealed chamber was filled with water. The chamber temperature was maintained at 45 °C (lipid-only GUVs) or 50 °C (hybrid GUVs) with an external heating element. A sinusoidal wave with an amplitude of 3 V was applied at a frequency of 10 Hz for 30 minutes; then, the frequency was reduced to 3 Hz for 15 minutes. After this, 2 V/1 Hz were applied for 7.5 minutes, and then 2 V/0.5 Hz for 7.5 minutes. Prior to collection of GUVs, the chamber was allowed to cool freely to room temperature, typically requiring roughly 90 minutes. GUVs were stored in a plastic conical tube and imaged the same day.

To prepare a sample for imaging, a small aliquot of GUV suspension was added to a chamber formed by a glass slide, vacuum grease, and no. 1.5 cover slip. Images were collected using a Nikon Eclipse 80i equipped with either a 60x oil immersion or 60x air objective. The air objective was used for all images collected above or below room temperature to avoid thermal coupling of the sample and objective. A heated microscope stage (BoliOptics) was used to control the sample temperature. Sample temperatures were recorded as the average of the temperatures at the upper surfaces of the cover slip and glass slide, as measured by two resistance temperature detectors (Minco). To assess transition temperatures, GUVs were heated to 5-10 °C above the expected transition temperature, then cooled in increments of 2 °C while far from the expected transition

temperature. The temperature was then reduced in increments of 1 °C as the expected transition temperature was approached. Lipid-only GUVs were allowed to equilibrate for a minimum of 7 minutes at each temperature, while hybrid GUVs were allowed at least 10 minutes. The transition temperature was identified as the temperature at which domains first appeared upon cooling. Experimental uncertainty in T<sub>m</sub> was determined to be roughly a range of 1.5 °C, based on repeated experiments with selected compositions of GUVs.

### 2.4 Collection and analysis of laurdan emission spectra

LUVs containing laurdan were prepared as described above, using a lipid:probe ratio of 200:1. The prepared LUVs were diluted with water to a final lipid concentration of 200 µM immediately prior to fluorescence spectroscopy experiments. Laurdan emission spectra were collected from 370-600 nm with a Jasco spectrofluorometer using an excitation wavelength of 355 nm. Samples were heated to the highest temperature of interest, allowed to equilibrate for 30 minutes, then cooled in increments of 2 °C with an incubation time of 3 minutes at each temperature. Each sample was subjected to only one heating/cooling cycle prior to being discarded.

Laurdan generalized polarization (GP) provides insight into membrane polarity, with higher GP values corresponding to a more polar membrane. GP values were calculated using Equation (1), where  $I_{440}$  and  $I_{490}$  are the respective intensities of the laurdan emission spectrum at 440 nm and 490 nm.

$$GP = \frac{I_{440} - I_{490}}{I_{440} + I_{490}} \tag{1}$$

Least squares regression was also applied to fit a sigmoidal equation to calculated GP values (Equation (2)) [18].  $GP_{max}$  and  $GP_{min}$  represent the upper and lower limits of the GP curve, while n is a fitting parameter related to the slope of the curve in the vicinity of  $T_{mid}$ .  $T_{mid}$  represents the inflection point of the curve. Uncertainty values for  $T_{mid}$  were expressed as the standard deviation error for the fitting of this parameter.

$$GP(T) = \frac{GP_{max} - GP_{min}}{1 + e^{(T - T_{mid})n}} + GP_{min}$$
(2)

Decomposition of laurdan emission spectra into multiple peaks was also carried out to gain further insight into membrane phase behavior. Emission spectra were fit in Python with the sum of multiple lognormal curves using least squares regression as described in Puff et al. [18], with each lognormal curve characterized by an equation of the following form:

$$y = A_0 + A_1 exp \left[ -\left(\frac{\ln\left(\frac{x}{A_2}\right)}{A_3}\right)^2 \right]$$
 (3)

 $A_0$  represents the baseline,  $A_1$  the amplitude,  $A_2$  the position, and  $A_3$  the width of the fitted curve. All parameters besides  $A_0$  were constrained to be greater than 0 when performing the fit. Additionally, the peak position  $A_2$  was constrained to the range of measured wavelengths, which spans the observed emission spectrum of laurdan in the membrane. Prior to spectral decomposition, emission intensities were expressed as a function of energy at each wavelength using the relationship  $(h^*c/E^2)$ , where h is Planck's constant, c is the speed of light in a vacuum, and E is the energy corresponding to each wavelength (calculated as  $h^*c/\lambda$ , where  $\lambda$  is the wavelength) [18,22,23].

When three-peak fits to laurdan emission spectra were used, peak area ratios were calculated at each temperature studied as the area of the middle energy peak divided by the area of the lowest energy peak unless otherwise specified. Peak area ratio plots were fit with a three-piece linear function in Python to identify the temperature at which the first two lines met, which is expected to be within the range the phase transition temperature of the membrane, as described in Puff et al [18]. Uncertainty values for this position were reported as the standard deviation error in the intersection of these lines as calculated from the standard deviation error of the piecewise linear fit applied to each peak area ratio plot.

### 3. Results and Discussion

A combination of fluorescence spectroscopy and microscopy was used to study phase behavior in large unilamellar vesicles (LUVs) and giant unilamellar vesicles (GUVs) composed of palmitoyl oleoyl phosphatidylcholine (POPC) or polybutadiene-*block*-polyethylene oxide (PBdPEO), egg sphingomyelin (egg SM), and cholesterol. Compositions are reported as mole percentages.

#### 3.1 Cholesterol-free vesicles

First, a selected 40-60 mol% composition of POPC-egg SM and PBdPEO-egg SM LUVs was compared. Calculating the generalized polarization (GP) of laurdan in these LUVs as described in Equation (1)yielded the plot in Figure 1A. Both curves display a sigmoidal dependence of GP on temperature, with the inflection point ( $T_{mid}$ ) of each curve representing the approximate midpoint temperature for the formation of solid phase domains [24]. For the POPC-egg SM LUVs, laurdan GP indicated a  $T_{mid}$  of 27.5±0.2 °C. For the PBdPEO-egg SM LUVs,  $T_{mid}$  was 33.9±0.2 °C. Figure 1B shows fluorescence images of 40-60 mol% POPC-egg SM and PBdPEO-egg SM GUVs. After heating GUVs so that a single phase was observed, dark domains formed upon cooling. The

temperature at which domains first appeared upon cooling  $(T_m)$ ,  $32.0\pm1.5$  °C for POPC-egg SM and  $33.0\pm1.5$  °C for PBdPEO-egg SM, was within a few degrees of  $T_{mid}$  measured by laurdan GP. In both cases, irregularly shaped domains were observed as shown in Figure 1B, indicative of solid/fluid phase separation.

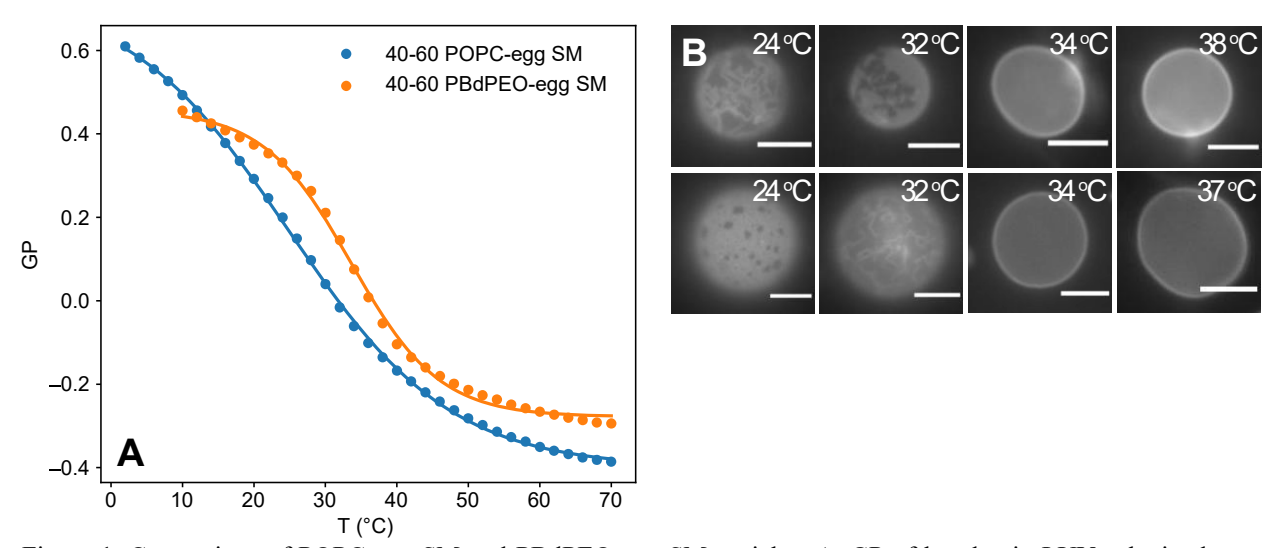


Figure 1. Comparison of POPC-egg SM and PBdPEO-egg SM vesicles. A. GP of laurdan in LUVs obtained upon cooling. The inflection point,  $T_{mid}$ , for the POPC-egg SM LUVs is  $27.5\pm0.2$  °C, and for the PBdPEO-egg SM LUVs is  $33.9\pm0.2$  °C. Plotted points show calculated GP values, while lines show a fit to Equation (2). B. Fluorescence microscopy of GUVs. Top row, 40-60 mol% POPC-egg SM GUVs; bottom row, 40-60 mol% PBdPEO-egg SM. The temperature at which domains in GUV populations first appeared upon cooling,  $T_{ms}$ , is  $32.0\pm1.5$  °C for the POPC-egg SM GUVs and  $33.0\pm1.5$  °C for the PBdPEO-egg SM GUVs. Scale bar is  $10~\mu m$ .

### 3.2 Analysis of laurdan spectroscopy results for POPC-egg SM-cholesterol LUVs

These methods were then applied to POPC-egg SM-cholesterol vesicles containing sufficient cholesterol to promote liquid/liquid phase separation. Laurdan GP values in POPC-egg SM-cholesterol LUVs are shown in Figure 2A. The shapes of the GP curves are generally sigmoidal, suggesting a phase transition takes place within the temperature range studied. However, the shallow slopes of the GP curves contrast especially with the results shown in Figure 1A for vesicles containing no cholesterol, for which a less broad phase transition is expected. This can make clear assessment of the inflection point difficult. For egg phosphatidylcholine-egg SM-cholesterol LUVs containing less cholesterol, good agreement between GP analysis and GUV phase transitions has been reported [18]. However, for the POPC-egg SM-cholesterol compositions shown in Figure 2A, the T<sub>mid</sub> values indicated by laurdan GP range from roughly 40-50 °C. These temperatures are significantly above the range of 20-35 °C expected for miscibility of the two liquid phases for similar vesicle compositions [9,18].

Decomposition of laurdan emission spectra into multiple peaks [18] was therefore carried out in an attempt to gain further insight into the phase behavior of cholesterol-containing membranes

beyond the information provided by GP values. Three lognormal peaks characterized by Equation (3) were used to fit laurdan emission spectra as described in Puff et al [18]. An example of such a decomposition for 30-40-30 mol% POPC-egg SM-chol at 20 °C is shown in Figure S1.

For the three-peak fits of laurdan emission spectra in POPC-egg SM-cholesterol vesicles, the peak positions typically ranged from ~2.89-2.92 eV (425-430 nm, high-eV peak), ~2.67-2.79 eV (445-465 nm, mid-eV peak), and ~2.48-2.58 eV (480-500 nm, low-eV peak) across the range of temperatures studied. This is comparable to the ranges reported for similar multipeak analyses of laurdan [18,25] and BADAN [26], a probe with the same fluorescent moiety as laurdan. These peaks are hypothesized to respectively correspond to a non-hydrogen bonded state, an immobilized hydrogen bonded state, and a mobile hydrogen bonded state [26]. The ratio of the areas of the mideV peak and low-eV peak has thus been proposed as a metric of the relative amount of the liquid ordered phase in cholesterol-containing vesicles [18].

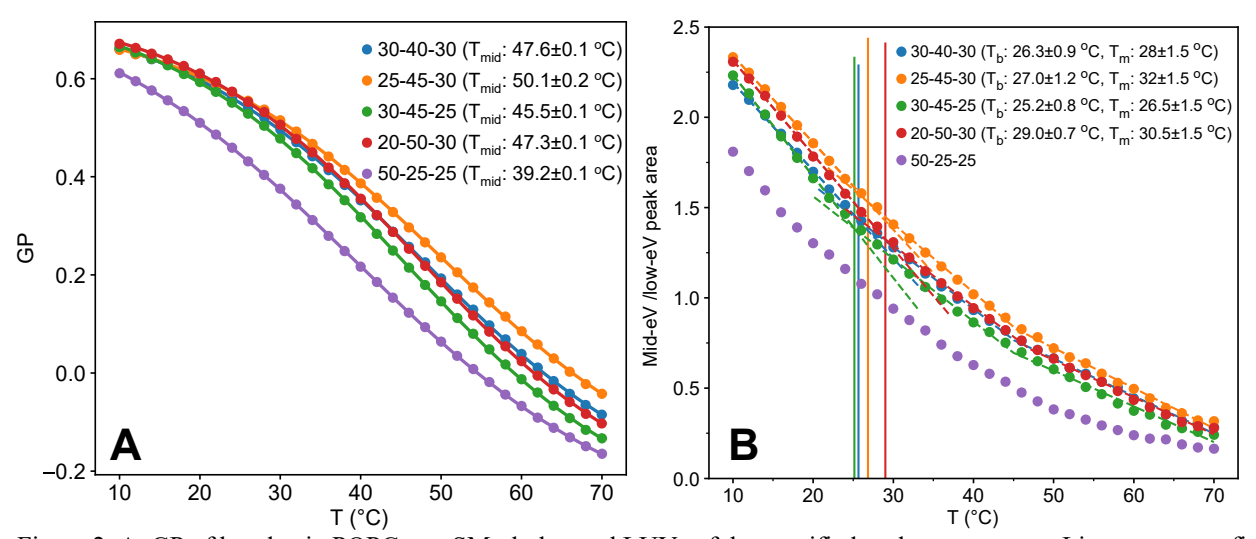


Figure 2. A. GP of laurdan in POPC-egg SM-cholesterol LUVs of the specified mole percentages. Lines represent fits to an equation for a sigmoidal curve, as described in Equation (2), and  $T_{mid}$  is the inflection point of this fit. B. Plot of the ratios of the mid-eV and low-eV peak areas resulting from the decomposition of laurdan emission spectrum into three peaks. Dashed lines indicate the piecewise linear function used to evaluate  $T_{break}$ . Vertical lines indicate  $T_{break}$ , the temperature at which the slope of the plot changes ( $T_b$  in the legend).  $T_m$  in the legend refers to the temperature at which domains first appeared upon cooling indicated by fluorescence microscopy images of GUVs.

The results of carrying out three-peak laurdan emission spectra decomposition for POPC-egg SM-cholesterol LUVs are therefore plotted in Figure 2B as the area of the mid-eV peak divided by the area of the low-eV peak [18]. As described in Puff et al. [18], this resulted in concave plots. A three-piece linear fit was applied to each plot, and the temperatures at which the first line and second line meet (T<sub>break</sub>, indicated by the vertical lines in Figure 2B) lie within the range of the miscibility transition expected based on previous literature [9,18]. Moreover, plotting these transitions as a heat map in Figure S2 on a 3-component triangle yielded expected trends [9]. Therefore, multipeak analysis may be a more accurate approach than GP analysis to interpreting this laurdan spectral data.

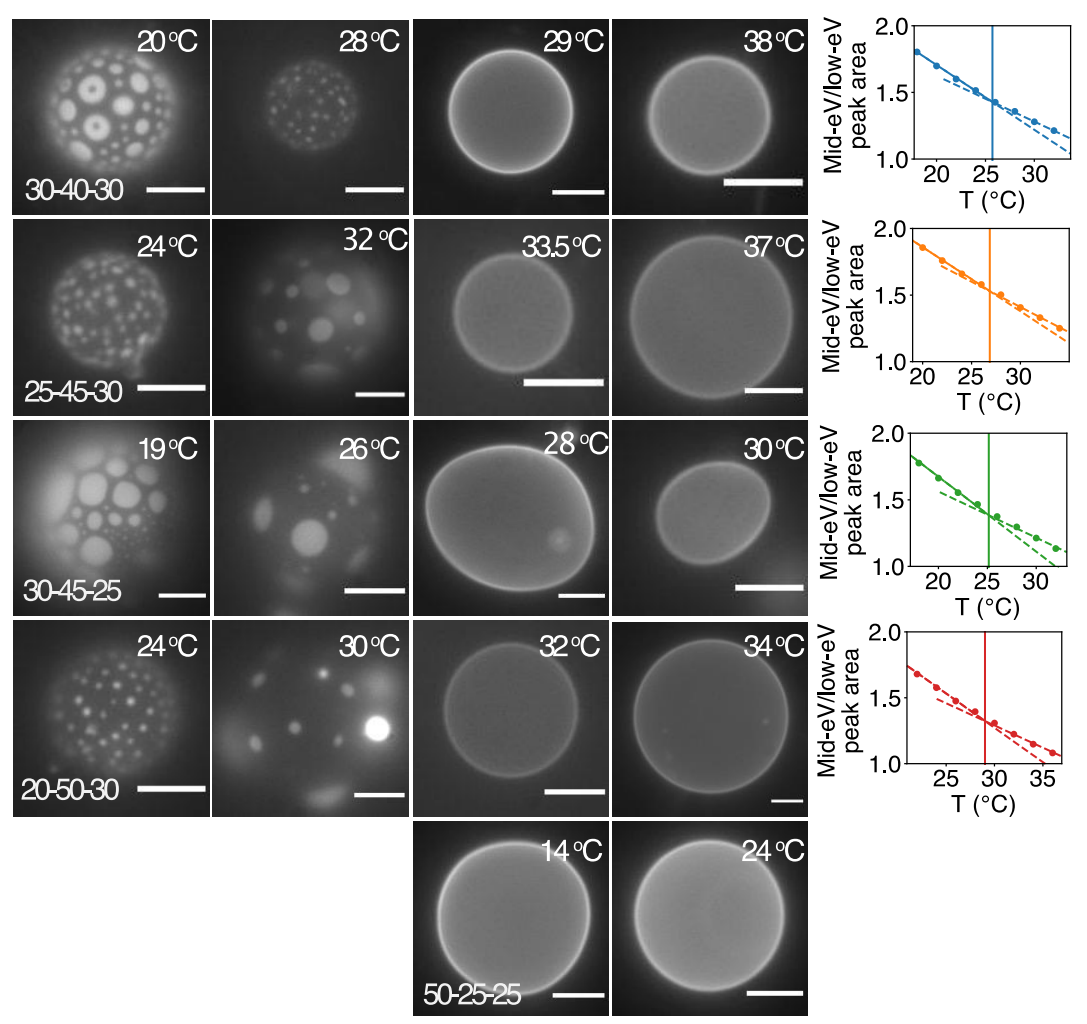


Figure 3. Fluorescence microscopy images of POPC-egg SM-cholesterol GUVs of the specified mole percentages across a range of temperatures. Some deformation of GUVs is evident at higher temperatures, likely due to a combination of the increased fluidity of the membrane and convection within the sample volume. Scale bar represents  $10 \, \mu m$ . Rightmost panels show portions of Figure 2B for individual compositions in the vicinity of  $T_{break}$ . Dashed lines indicate the piecewise linear function used to evaluate  $T_{break}$ . Vertical line denotes  $T_{break}$ 

# 3.3 POPC-egg SM-cholesterol GUV behavior

For comparison, GUVs of the same compositions were examined, as shown in Figure 3. The temperatures at which domains first appeared upon cooling (T<sub>m</sub>) were in good agreement with T<sub>break</sub> (see plots in Figure 3, and Table S1) but not T<sub>mid</sub> laurdan GP results (see legends of Figure 2). T<sub>m</sub> values were also in good agreement with previously published work regarding GUVs composed of a similar lipid mixture (which instead incorporated palmitoyl sphingomyelin (PSM), the primary component of egg SM) [9]. GUVs typically displayed bright, round domains on a dark background, suggesting the presence of both the liquid disordered (POPC-rich) and liquid ordered (egg SM-rich) phases. For the 50-25-25 mol% POPC-egg SM-cholesterol GUVs, domains were

not observed at room temperature or at the lowest temperature accessible to us (~13 °C). This composition lies at the very edge of the previously reported two-phase region for POPC-PSM-cholesterol GUVs [9], so it is possible the slight compositional differences between egg SM and PSM may have resulted in the observation of only one phase for this composition.

# 3.4 Analysis of laurdan spectroscopy results for PBdPEO-egg SM-cholesterol LUVs

Given the consistent results of the three-peak decomposition for lipid-only membranes containing cholesterol (i.e., good agreement of T<sub>break</sub> with T<sub>m</sub>), we then applied the same approach to hybrid membranes containing the block copolymer polybutadiene-*block*-polyethylene oxide instead of POPC. Results of laurdan GP calculation and laurdan emission spectrum decomposition are shown in Figure 4. As for the POPC-egg SM-cholesterol vesicles, the shallow slopes of the laurdan GP curves suggest a broad phase transition. T<sub>mid</sub> values ranged from ~35-56 °C (legend of Figure 4A) by fitting to Equation (2), similar to those indicated by laurdan GP for POPC-egg SM-cholesterol LUVs.

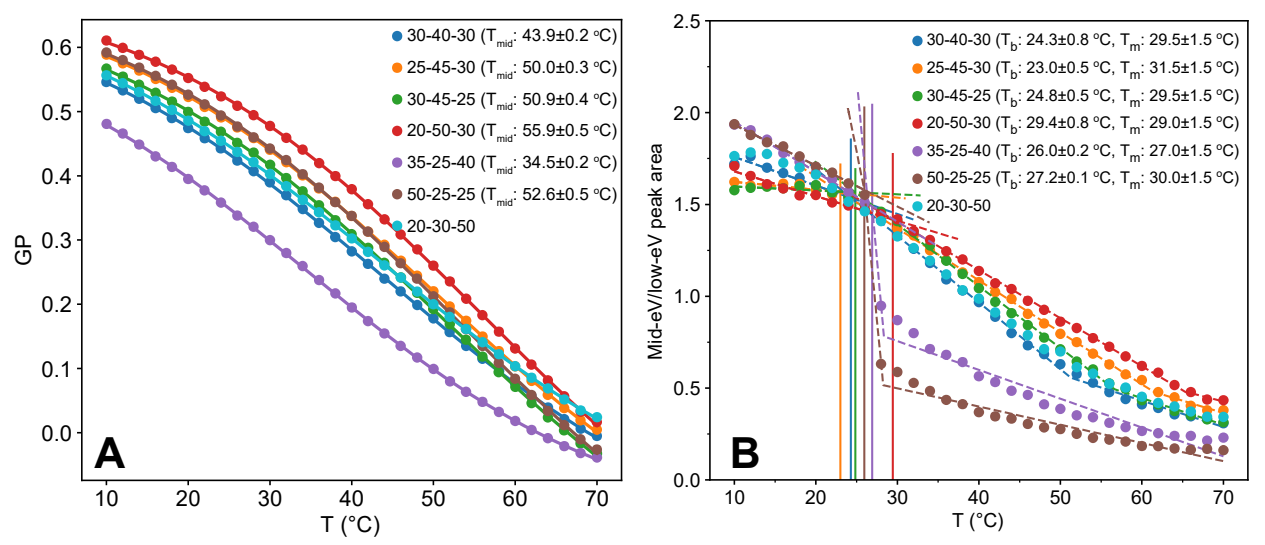


Figure 4. A. GP of laurdan in PBdPEO-egg SM-chol LUVs of the specified mole percentages.  $T_{mid}$  is the inflection point indicated by fitting to Equation (2). B. Ratio of the areas beneath the mid-eV and low-eV peaks resulting from the decomposition into three curves of laurdan emission spectra in PBdPEO-egg SM-chol LUVs of the specified mole percentages. Vertical lines indicate the first change in slope at temperature  $T_{break}$ . In the legend,  $T_b$  refers to  $T_{break}$ .  $T_m$  in the legend refers to the temperature at which domains first appeared upon cooling indicated by fluorescence microscopy images of GUVs. Dashed lines indicate the piecewise linear function used to evaluate  $T_{break}$ .

Figure S3 shows an example of a three-peak fit to a laurdan emission spectrum for 30-40-30 mol% PBdPEO-egg SM-chol at 20 °C. The small values of the residuals and relatively Gaussian distribution suggest a good fit is achieved with three peaks. A difference in the shapes of the peak area ratio profiles is clear between the hybrid (Figure 4B) and lipid-only (Figure 2B) membranes. While the lipid-only membranes had concave peak area ratio plots, those for the hybrid membranes appeared roughly sigmoidal, with some compositions displaying a discontinuity at T<sub>break</sub> and others

displaying a change in slope. Additionally, T<sub>break</sub> values were in a similar range, ~23-29 °C (legend of Figure 4B), to those indicated for POPC-egg SM-cholesterol LUVs.

To further investigate, peak area ratio plots were constructed for a broad range of compositions of hybrid LUVs (Figure 5). At T<sub>break</sub>, either a discontinuity (Figure 5A) or only a change in slope (Figure 5B) was observed depending on the composition. The peak area ratio is expected to correlate with the relative amount of the liquid ordered phase—more specifically, with the relative amount of hydrogen-bound but immobile laurdan [18,26]. This suggests that for the compositions plotted in Figure 5A, once the temperature decreases below T<sub>break</sub>, the liquid-ordered lipid population increases sharply. For the compositions in Figure 5B, after the temperature decreases below T<sub>break</sub>, the size of this population increases gradually.

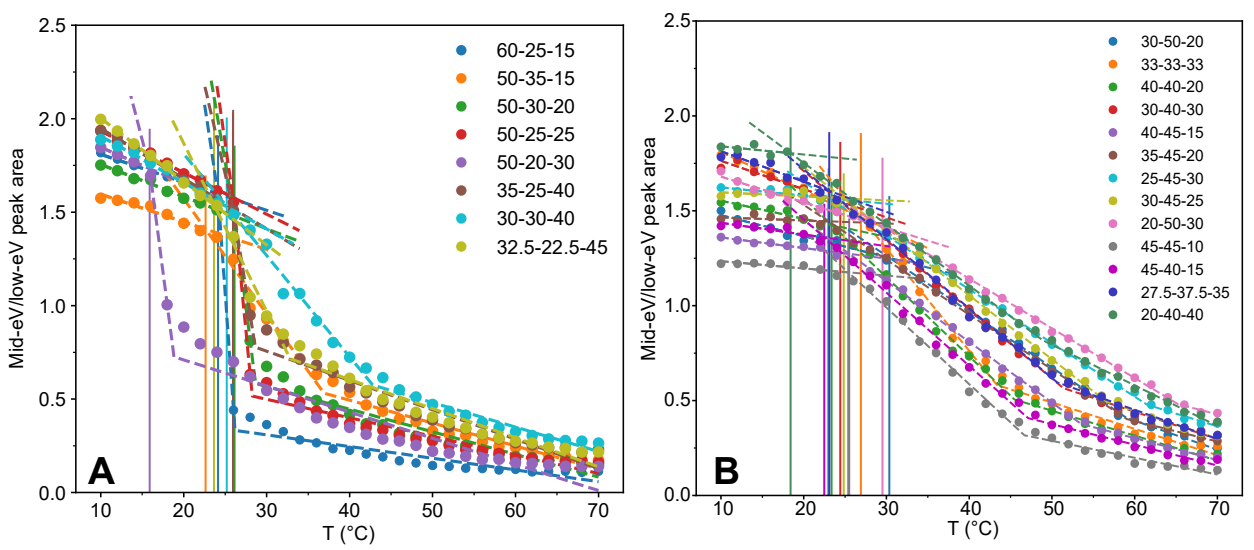


Figure 5. Comparison of trends in the temperature dependence of the peak area ratio plots for PBdPEO-egg SM-chol LUVs of the specified mole percentages. Dashed lines indicate the piecewise linear function used to evaluate  $T_{break}$ . A. Compositions for which the peak area ratio plot shows a discontinuity at  $T_{break}$ . B. Compositions for which the peak area ratio plot shows only a change in slope at  $T_{break}$ .

To better visualize any compositional trends in T<sub>break</sub> and in the peak area ratio plots for hybrid LUVs, a 3-component triangle (Figure 6A) was used. T<sub>break</sub> values are plotted as a heat map on the 3-component triangle. In Figure 6A, red circles indicate compositions displaying a discontinuity in their peak area ratio plot. This is not a phase diagram, as the results are not shown at a single temperature, but instead represents an overview of the data presented above. For comparison, a similar figure was constructed for the POPC-egg SM-cholesterol LUVs discussed above (Figure S2).

The  $T_{break}$  values shown on the heat maps in Figure 6 tend to increase as the amount of egg SM is increased and the amount of cholesterol is decreased, similar to the trends reported for lipid vesicles [9]. The range of temperatures observed for  $T_{break}$  (~15-30 °C for the compositions studied here) is also similar to the miscibility transitions reported in POPC-PSM-cholesterol GUVs of

comparable compositions [9]. For the hybrid vesicles, however, T<sub>break</sub> is significantly higher at high cholesterol contents (>30%) indicating relatively less miscibility between PBdPEO and egg SM. In this respect, some similarity is shared with the phase coexistence region of dioleoylphosphatidylcholine (DOPC)-PSM-cholesterol vesicles, which displays miscibility temperature values near room temperature at ~40 mol% cholesterol [9].

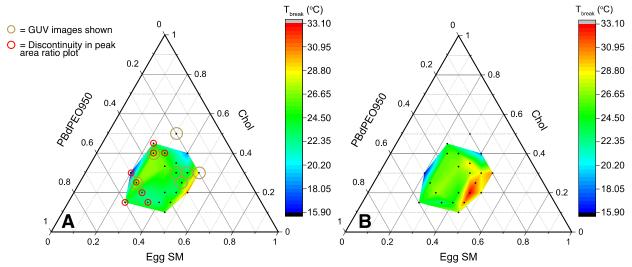


Figure 6. Heat maps of T<sub>break</sub> values indicated by laurdan in PBdPEO-egg SM-cholesterol LUVs. A. T<sub>break</sub> values calculated from the ratio of the mid-eV and low-eV peak areas. Gold circles mark compositions for which images of GUVs are shown. Compositions for which a discontinuity is observed in the laurdan peak area ratio plots are indicated with a red circle. For the single point plotted outside the edges of the heat map, only a single phase was observed for GUVs at the lowest accessible temperature (~13 °C). However, the edges of the heat map do not indicate the boundaries of a phase coexistence region. B. T<sub>break</sub> values recalculated based on the ratio of the mid-eV peak area to the sum of the areas of all three peaks. T<sub>break</sub> was obtained from the meeting point of the first and second lines of a piecewise linear fit to the peak area ratios, as in part A.

For two-phase lipid GUVs, phase separation by spinodal decomposition has been reported for compositions with the average area fraction of one phase ranging from 0.3-0.7 (i.e., similar proportions of each phase) [27]. Outside of this range, phase separation is initiated by nucleation and growth, which takes place when there is a discontinuity in the composition associated with the new phase. Therefore, it is not too surprising that the compositions for which a discontinuity in the peak area ratio plot was observed are all positioned roughly on the left side of the phase space explored, which is perhaps in the compositional range for nucleation and growth. The lack of discontinuities in the peak area ratio plots for the remainder of the compositions suggests that they phase separate by spinodal composition, which may be visible somewhat in the domain morphologies observed in GUVs.

### 3.5 PBdPEO-egg SM-cholesterol GUVs and further analysis of laurdan spectroscopy results

For comparison, GUVs of compositions from Figure 4 were imaged. The temperatures at which domains first appeared upon cooling  $(T_m)$  were in better agreement with  $T_{break}$  than with the  $T_{mid}$  laurdan results (see legends of Figure 4). To attempt to gain better agreement between  $T_{break}$  and

 $T_m$ , an additional fitting approach was used. The relative amount of the mid-eV peak, reported to be correlated with the relative abundance of the liquid ordered phase [18], was recalculated by comparing the area of the mid-eV peak to the area of all three peaks (Table S2). Interestingly, this resulted in better agreement for the compositions with larger ( $\sim$ >4-5 °C) discrepancies between  $T_{break}$  and  $T_m$ . For the compositions for which there was little difference between  $T_{break}$  and  $T_m$ , this recalculation did not significantly change  $T_{break}$  (typically less than a  $\sim$ 1 °C difference after recalculation).

For the hybrid membranes, certain compositions displayed a high-eV peak area that remained relatively consistent at all temperatures studied, both above and below T<sub>m</sub> in GUVs. In comparison, for the lipid-only vesicles in this work the area beneath the high-eV peak increased and the area beneath the low-eV peak decreased as the temperature decreased (Figure S4), consistent with the expectation of an increasingly ordered membrane at lower temperatures and with previously reported results [18,19]. DOPC vesicles [19] also unexpectedly displayed high energy peaks of relatively constant area with temperature in another work. The authors attributed the relatively constant area of these peaks to the presence of an energetically unfavorable but still observable population of non-hydrogen bonded laurdan molecules at high temperature, based on their report of a short lifetime at this wavelength. It is possible that such a phenomenon is taking place in the hybrid membranes as well. In such a case, considering the recalculation of the peak area ratios as described above may provide more accurate insight into the phase transition temperatures of hybrid vesicles.

Recalculating peak area ratios as the area of the mid-eV peak divided by the sum of the areas of the high-eV, mid-eV, and low-eV peaks and evaluating  $T_{break}$  resulted in the heat map shown in Figure 6B. Similar trends are observed for vesicles containing lower amounts of egg SM as shown in Figure 6A. However, for vesicles incorporating more than ~40% egg SM, recalculated  $T_{break}$  values were ~5-7 °C higher, which is more consistent with the trends observed for  $T_m$  in GUVs.

It should also be noted that below T<sub>m</sub>, it was typically more common to observe bright, single phase GUVs when PBdPEO rather than POPC was incorporated. This may be due to budding away of the dark phase prior to imaging; significant and rapid budding has been previously reported in hybrid GUVs incorporating a different triblock copolymer [28]. Therefore, discrepancies in T<sub>m</sub> and T<sub>break</sub> may also occur from differences in composition of hybrid GUVs and LUVs respectively attributed to rapid budding before the heating and cooling cycle. Alternatively, such compositional variations could arise from incomplete detachment of GUVs immediately after formation but prior to cooling [29–31]. This would allow domain formation in the interconnected GUV buds prior to their separation and collection, resulting in subsequent compositional differences amongst individual GUVs.

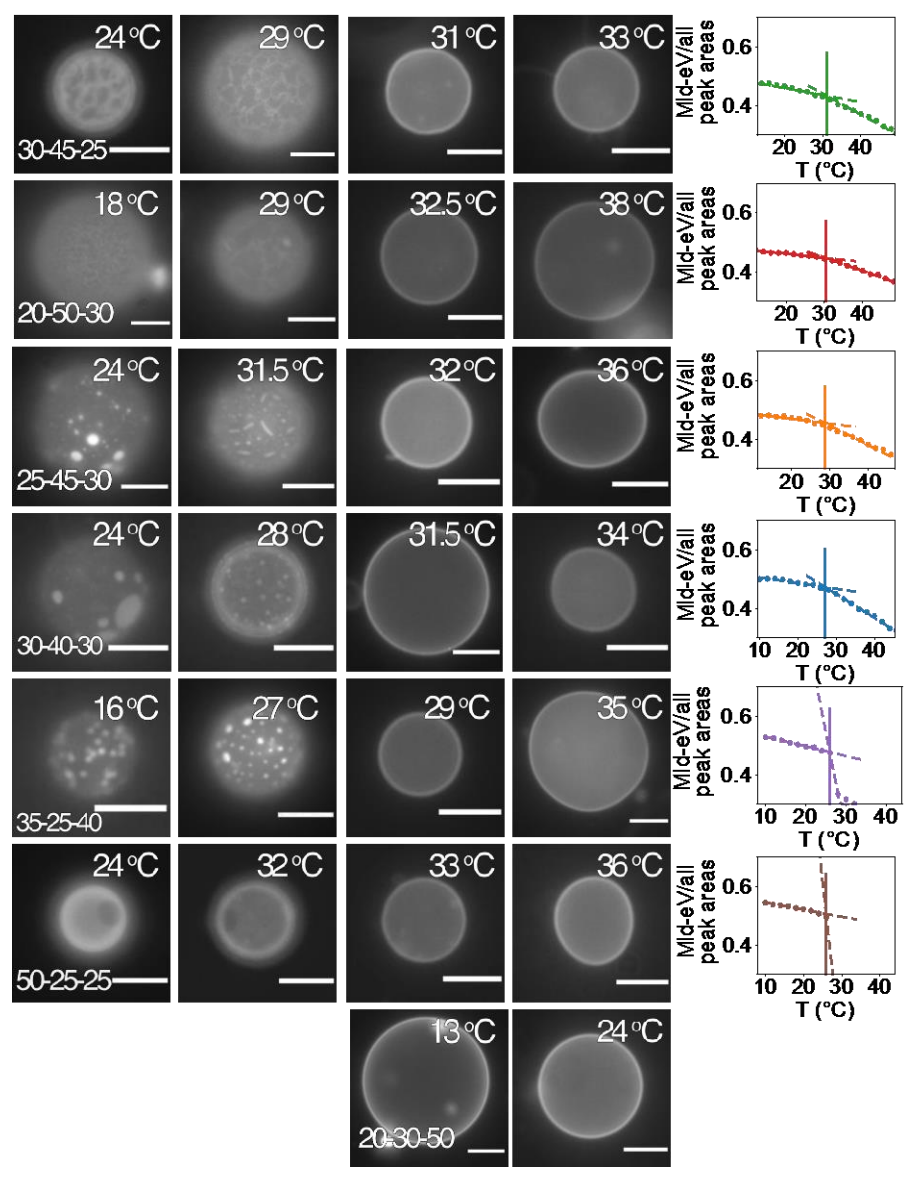


Figure 7. Fluorescence microscopy images of giant unilamellar vesicles consisting of PBdPEO-egg SM-cholesterol at the specified mole percentages across a range of temperatures. For the vesicles containing 50 mol% cholesterol, domains were not observed even at the lowest accessible temperature. For the 50-25-25 mol% sample,  $T_m$  was assessed by heating rather than cooling the vesicles, as excessive budding away of domains upon cooling complicated assessment of  $T_m$ . Scale bar represents 10  $\mu$ m. Rightmost panels show portions of peak area ratio plots recalculated by dividing the area of the mid-eV peak by the sum of the areas of all three peaks for individual compositions in the vicinity of  $T_{break}$ . Dashed lines indicate the piecewise linear function used to evaluate  $T_{break}$ . Vertical line denotes  $T_{break}$ .

Fluorescence images of GUVs of compositions from Figure 4 are shown in Figure 7. The panels on the far right of Figure 7 show selected regions of mid eV/all eV peaks near the refitted T<sub>break</sub> values for each composition. The compositions in rows 3-6 of Figure 7 (25-45-30, 30-40-30, 35-25-40, and 50-25-25 mol% PBdPEO-egg SM-cholesterol) appear to display coexisting fluid phases, based on the presence of round domains. In this case, the dark phase is likely rich in egg SM, given that below T<sub>m</sub> this dark phase makes up the majority of the vesicle surface area for

compositions richer in egg SM and less of the surface area when less egg SM is included. Circular domains have been previously reported in hybrid membranes upon inclusion of cholesterol and were hypothesized to be a liquid ordered-like phase [10].

In contrast to POPC-egg SM-cholesterol GUVs of the same compositions (Figure 3), the GUVs in rows 1 and 2 of Figure 7 (30-45-25 and 20-50-30 mol% PBdPEO-egg SM-cholesterol) appear to display predominantly solid/fluid instead of fluid/fluid phase separation, based on the irregularity of the domain shapes. This indicates greater amounts of cholesterol may be required to induce fluid/fluid phase separation in hybrid membranes as compared to lipid membranes. This result suggests that cholesterol partitions to a greater extent into PBdPEO in comparison to fluid lipids such as POPC. Of note, for POPC-PSM-cholesterol compositions with greater amounts of PSM, a three-phase region consisting of solid, liquid ordered, and liquid disordered phases with an upper bound delineated by the observed transition from fluid/fluid to solid/fluid phase separation has been suggested to exist across a range of cholesterol concentrations (~10-25 mol%) [9]. It is possible that one or both of the compositions of the GUVs in rows 1 and 2 of Figure 7 may lie within such a three-phase region as well, with T<sub>break</sub> perhaps corresponding to the appearance of the liquid-ordered phase as the sample is cooled.

For the 20-30-50 mol% PBdPEO-egg SM-cholesterol GUVs, no phase separated vesicles were observed at 13 °C or above, consistent with the observation that greater amounts of cholesterol were required to induce fluid/fluid phase separation in hybrid membranes than in lipid-only membranes. For comparison, a phase diagram for POPC-PSM-cholesterol GUVs indicates a single fluid phase exists above ~35 mol % cholesterol at temperatures greater than 15 °C [9]. Similarly, while 50-25-25 mol% PBdPEO-egg SM-cholesterol GUVs displayed dark, round domains up to ~32 °C, phase separation was not observed for POPC-egg SM-cholesterol GUVs of the same composition at or above ~13 °C, the lowest accessible temperature (Figure 3).

Rows 2-3 of Figure 7 (20-50-30 and 25-45-30 mol% PBdPEO-egg SM-cholesterol) show hybrid GUVs that displayed domain morphologies suggestive of spinodal decomposition below T<sub>m</sub>. For the 20-50-30 mol% GUVs, at low temperatures the widespread, grainy appearance of the domains and the low contrast between light and dark phases resemble the early stages of spinodal decomposition. Similarly, for the 25-45-30 mol% PBdPEO-egg SM-cholesterol GUVs elongation of domains is observed just below T<sub>m</sub>. Such morphologies have been observed in GUVs undergoing spinodal decomposition [7,32] and are attributed to reduced line tension near a critical point [7]. Additionally, these GUVs as well as those in rows 1 and 4 of Figure 7 (30-45-25 and 30-40-30 mol% PBdPEO-egg SM-cholesterol) display relatively low contrast in the brightness of light and dark domains—especially just below T<sub>m</sub>. This is indicative of a gradual change in composition, and thus weak partitioning of the probe. In agreement with these observations, these mixtures fall within the compositional region that was hypothesized to phase separate by gradual spinodal decomposition based upon laurdan multipeak analysis.

Of note, the length scales of the domains observed in GUVs and in LUVs are inherently different. Fluorescence microscopy enables observation of micron-scale domains in GUVs. While there may be temperatures at which stable nanodomains exist in GUVs but for some reason do not coalesce, this phenomenon occurs at a length scale unresolvable by fluorescence microscopy. LUVs, however, have diameters of ~100 nm; any domains that form in LUVs accordingly have sizes on the order of 100 nm or less. The laurdan experiments performed with LUVs would therefore detect the formation of such nanoscale domains. Theoretically, the same laurdan experiments could be carried out using GUVs, although our preliminary attempts to do so were limited by the low concentration of GUVs in solution yielded by electroformation. Further optimization of such experiments could allow for comparison between spectroscopy and microscopy results in GUVs.

To gauge the possible usefulness of multipeak analysis applied to cholesterol-free membranes, T<sub>break</sub> was evaluated for 40-60 mol% PBdPEO-egg SM vesicles based on the ratio of areas of the mid-eV peaks to the sum of the areas of all three peaks (Figure S5). A discontinuity in the vicinity of T<sub>break</sub> was observed, suggesting a significant difference in the compositions of the solid and fluid phases at T<sub>break</sub>. T<sub>break</sub> was 29.6±0.4 °C, less than both the GP T<sub>mid</sub> of 33.9±0.2 °C and the GUV T<sub>m</sub> of 33.0±1.5 °C. T<sub>break</sub> resulting from analysis of the ratios of the areas of the mid-eV and low-eV peaks for 40-60 mol% POPC-egg SM vesicles (Figure S5) was 36.7±0.8 °C, greater than both the GP T<sub>mid</sub> of 27.5±0.2 °C and the GUV T<sub>m</sub> of 32.0±1.5 °C. For POPC-egg SM LUVs, a gradual change in slope is observed in the vicinity of T<sub>break</sub>, similar to the trends observed for POPC-egg SM-cholesterol LUVs and suggestive of more gradual changes in the compositions of the two phases as the temperature is decreased. For cholesterol-free vesicles, which undergo a solid to fluid phase transition, laurdan GP analysis could potentially be used to more accurately determine the temperature at which solidification begins and the temperature at which half of the lipids have transitioned to the solid phase, as described in our previous work [16]. GUV T<sub>m</sub> values would then be expected to lie within the range of these temperatures. Conversely, multipeak analysis of laurdan emission spectra indicates a single temperature, T<sub>break</sub>. This may correspond more accurately to the behavior observed for GUVs in which the liquid ordered phase is present, typically resulting in domains that coalesce rapidly even just below T<sub>m</sub>.

### 4. Conclusions

Fluorescence spectroscopy and microscopy were employed to study the phase behavior of POPC-egg SM-cholesterol and PBdPEO-egg SM-cholesterol vesicles. While laurdan GP indicated phase behavior consistent with observations of GUVs for POPC-egg SM and PBdPEO-egg SM vesicles, multipeak analysis of laurdan emission spectra was found to provide more accurate insight into phase behavior than analysis of laurdan GP values for cholesterol-containing lipid-only and hybrid vesicles. For hybrid vesicles, taking the ratio of the area of the middle energy peak to the sum of the areas of all peaks improved the temperature-dependent agreement with GUV behavior in

comparison to the ratio of the area of the middle peak to the area of the lowest energy peak. Either a more gradual change in slope or a discontinuity around the break-point of this ratio was observed for the hybrid vesicles. We hypothesize that these trends correspond to the mechanism by which phase separation proceeds (spinodal decomposition or nucleation and growth) based on the characteristic shapes of the peak area ratio plots, the compositions for which each profile was observed, and the morphologies of domains in GUVs of corresponding compositions. The relatively high T<sub>break</sub> values at cholesterol contents greater than 30 mol% are suggestive of low miscibility of PBdPEO and egg SM. Additionally, greater amounts of cholesterol were observed to be required to induce fluid/fluid phase separation in hybrid GUVs than in lipid-only GUVs. This suggests stronger partitioning of cholesterol into PBdPEO than into POPC. These results, which we summarized on a heat map, may inform the further investigation of the phase behavior of hybrid vesicles toward applications such as drug delivery.

# Acknowledgements

This material is based upon work supported by the National Science Foundation under Grant No. DMR – 1806366.

# Appendix A. Supplementary data

Supplementary data to this article can be found online.

### **References:**

- [1] D. Chen, M.M. Santore, Hybrid copolymer–phospholipid vesicles: phase separation resembling mixed phospholipid lamellae, but with mechanical stability and control, Soft Matter. 11 (2015) 2617–2626. https://doi.org/10.1039/C4SM02502D.
- [2] S. Khan, M. Li, S.P. Muench, L.J.C. Jeuken, P.A. Beales, Durable proteo-hybrid vesicles for the extended functional lifetime of membrane proteins in bionanotechnology, Chem. Commun. 52 (2016) 11020–11023. https://doi.org/10.1039/C6CC04207D.
- [3] M.L. Jacobs, M.A. Boyd, N.P. Kamat, Diblock copolymers enhance folding of a mechanosensitive membrane protein during cell-free expression, PNAS. 116 (2019) 4031–4036. https://doi.org/10.1073/pnas.1814775116.
- [4] Z. Cheng, D.R. Elias, N.P. Kamat, E.D. Johnston, A. Poloukhtine, V. Popik, D.A. Hammer, A. Tsourkas, Improved Tumor Targeting of Polymer-Based Nanovesicles Using Polymer-Lipid Blends, Bioconjugate Chem. 22 (2011) 2021–2029. https://doi.org/10.1021/bc200214g.
- [5] Z.I. Imam, L.E. Kenyon, G. Ashby, F. Nagib, M. Mendicino, C. Zhao, A.K. Gadok, J.C. Stachowiak, Phase-Separated Liposomes Enhance the Efficiency of Macromolecular Delivery to the Cellular Cytoplasm, Cel. Mol. Bioeng. 10 (2017) 387–403. https://doi.org/10.1007/s12195-017-0489-4.
- [6] A.N. Trementozzi, Z.I. Imam, M. Mendicino, C.C. Hayden, J.C. Stachowiak, Liposome-Mediated Chemotherapeutic Delivery is Synergistically Enhanced by Ternary Lipid Compositions and Cationic Lipids, Langmuir. 35 (2019) 12532–12542. https://doi.org/10.1021/acs.langmuir.9b01965.

- [7] S.L. Veatch, S.L. Keller, Seeing spots: Complex phase behavior in simple membranes, Biochimica et Biophysica Acta (BBA) Molecular Cell Research. 1746 (2005) 172–185. https://doi.org/10.1016/j.bbamcr.2005.06.010.
- [8] D. Marsh, Cholesterol-induced fluid membrane domains: A compendium of lipid-raft ternary phase diagrams, Biochimica et Biophysica Acta (BBA) Biomembranes. 1788 (2009) 2114–2123. https://doi.org/10.1016/j.bbamem.2009.08.004.
- [9] S.L. Veatch, S.L. Keller, Miscibility Phase Diagrams of Giant Vesicles Containing Sphingomyelin, Phys. Rev. Lett. 94 (2005) 148101. https://doi.org/10.1103/PhysRevLett.94.148101.
- [10] J. Nam, T.K. Vanderlick, P.A. Beales, Formation and dissolution of phospholipid domains with varying textures in hybrid lipo-polymersomes, Soft Matter. 8 (2012) 7982–7988. https://doi.org/10.1039/c2sm25646k.
- [11] S. Winzen, M. Bernhardt, D. Schaeffel, A. Koch, M. Kappl, K. Koynov, K. Landfester, A. Kroeger, Submicron hybrid vesicles consisting of polymer lipid and polymer cholesterol blends, Soft Matter. 9 (2013) 5883–5890. https://doi.org/10.1039/C3SM50733E.
- [12] B.R. Lentz, Y. Barenholz, T.E. Thompson, Fluorescence depolarization studies of phase transitions and fluidity in phospholipid bilayers. 2. Two-component phosphatidylcholine liposomes, Biochemistry. 15 (1976) 4529–4537. https://doi.org/10.1021/bi00665a030.
- [13] T. Parasassi, G. De Stasio, G. Ravagnan, R.M. Rusch, E. Gratton, Quantitation of lipid phases in phospholipid vesicles by the generalized polarization of Laurdan fluorescence, Biophysical Journal. 60 (1991) 179–189. https://doi.org/10.1016/S0006-3495(91)82041-0.
- [14] W.F. Zeno, S. Hilt, K.K. Aravagiri, S.H. Risbud, J.C. Voss, A.N. Parikh, M.L. Longo, Analysis of Lipid Phase Behavior and Protein Conformational Changes in Nanolipoprotein Particles upon Entrapment in Sol-Gel-Derived Silica, Langmuir. 30 (2014) 9780–9788. https://doi.org/10.1021/la5025058.
- [15] K. Suga, H. Umakoshi, Detection of Nanosized Ordered Domains in DOPC/DPPC and DOPC/Ch Binary Lipid Mixture Systems of Large Unilamellar Vesicles Using a TEMPO Quenching Method, Langmuir. 29 (2013) 4830–4838. https://doi.org/10.1021/la304768f.
- [16] N. Hamada, S. Gakhar, M.L. Longo, Hybrid lipid/block copolymer vesicles display broad phase coexistence region, Biochimica et Biophysica Acta (BBA) Biomembranes. 1863 (2021) 183552. https://doi.org/10.1016/j.bbamem.2021.183552.
- [17] K. Flandez, S. Bonardd, M. Soto-Arriaza, Physicochemical properties of L-alpha dipalmitoyl phosphatidylcholine large unilamellar vesicles: Effect of hydrophobic block (PLA/PCL) of amphipathic diblock copolymers, Chemistry and Physics of Lipids. 230 (2020) 104927. https://doi.org/10.1016/j.chemphyslip.2020.104927.
- [18] N. Puff, G. Staneva, M.I. Angelova, M. Seigneuret, Improved Characterization of Raft-Mimicking Phase-Separation Phenomena in Lipid Bilayers Using Laurdan Fluorescence with Log-Normal Multipeak Analysis, Langmuir. 36 (2020) 4347–4356. https://doi.org/10.1021/acs.langmuir.0c00412.
- [19] N. Watanabe, Y. Goto, K. Suga, T.K.M. Nyholm, J.P. Slotte, H. Umakoshi, Solvatochromic Modeling of Laurdan for Multiple Polarity Analysis of Dihydrosphingomyelin Bilayer, Biophysical Journal. 116 (2019) 874–883. https://doi.org/10.1016/j.bpj.2019.01.030.
- [20] M. Bacalum, B. Zorilă, M. Radu, Fluorescence spectra decomposition by asymmetric functions: Laurdan spectrum revisited, Anal Biochem. 440 (2013) 123–129. https://doi.org/10.1016/j.ab.2013.05.031.

- [21] J.C.-M. Lee, M. Santore, F.S. Bates, D.E. Discher, From Membranes to Melts, Rouse to Reptation: Diffusion in Polymersome versus Lipid Bilayers, Macromolecules. 35 (2002) 323–326. https://doi.org/10.1021/ma0112063.
- [22] J. Mooney, P. Kambhampati, Get the Basics Right: Jacobian Conversion of Wavelength and Energy Scales for Quantitative Analysis of Emission Spectra, J. Phys. Chem. Lett. 4 (2013) 3316–3318. https://doi.org/10.1021/jz401508t.
- [23] A.D. Lúcio, C.C. Vequi-Suplicy, R.M. Fernandez, M.T. Lamy, Laurdan Spectrum Decomposition as a Tool for the Analysis of Surface Bilayer Structure and Polarity: a Study with DMPG, Peptides and Cholesterol, J Fluoresc. 20 (2010) 473–482. https://doi.org/10.1007/s10895-009-0569-5.
- [24] B. Kubsch, T. Robinson, R. Lipowsky, R. Dimova, Solution Asymmetry and Salt Expand Fluid-Fluid Coexistence Regions of Charged Membranes, Biophysical Journal. 110 (2016) 2581–2584. https://doi.org/10.1016/j.bpj.2016.05.028.
- [25] N. Watanabe, K. Suga, J.P. Slotte, T.K.M. Nyholm, H. Umakoshi, Lipid-Surrounding Water Molecules Probed by Time-Resolved Emission Spectra of Laurdan, Langmuir. 35 (2019) 6762–6770. https://doi.org/10.1021/acs.langmuir.9b00303.
- [26] R.B.M. Koehorst, R.B. Spruijt, M.A. Hemminga, Site-Directed Fluorescence Labeling of a Membrane Protein with BADAN: Probing Protein Topology and Local Environment, Biophysical Journal. 94 (2008) 3945–3955. https://doi.org/10.1529/biophysj.107.125807.
- [27] C.A. Stanich, A.R. Honerkamp-Smith, G.G. Putzel, C.S. Warth, A.K. Lamprecht, P. Mandal, E. Mann, T.-A.D. Hua, S.L. Keller, Coarsening Dynamics of Domains in Lipid Membranes, Biophysical Journal. 105 (2013) 444–454. https://doi.org/10.1016/j.bpj.2013.06.013.
- [28] T.P.T. Dao, F. Fernandes, E. Ibarboure, K. Ferji, M. Prieto, O. Sandre, J.-F. Le Meins, Modulation of phase separation at the micron scale and nanoscale in giant polymer/lipid hybrid unilamellar vesicles (GHUVs), Soft Matter. 13 (2017) 627–637. https://doi.org/10.1039/C6SM01625A.
- [29] D.J. Estes, M. Mayer, Giant liposomes in physiological buffer using electroformation in a flow chamber, Biochimica et Biophysica Acta (BBA) Biomembranes. 1712 (2005) 152–160. https://doi.org/10.1016/j.bbamem.2005.03.012.
- [30] A. Li, J. Pazzi, M. Xu, A.B. Subramaniam, Cellulose Abetted Assembly and Temporally Decoupled Loading of Cargo into Vesicles Synthesized from Functionally Diverse Lamellar Phase Forming Amphiphiles, Biomacromolecules. 19 (2018) 849–859. https://doi.org/10.1021/acs.biomac.7b01645.
- [31] J. Pazzi, A.B. Subramaniam, Nanoscale Curvature Promotes High Yield Spontaneous Formation of Cell-Mimetic Giant Vesicles on Nanocellulose Paper, ACS Appl. Mater. Interfaces. 12 (2020) 56549–56561. https://doi.org/10.1021/acsami.0c14485.
- [32] S.L. Veatch, S.L. Keller, Separation of Liquid Phases in Giant Vesicles of Ternary Mixtures of Phospholipids and Cholesterol, Biophysical Journal. 85 (2003) 3074–3083. https://doi.org/10.1016/S0006-3495(03)74726-2.

Characterization of phase separation phenomena in hybrid lipid/block copolymer/cholesterol bilayers using laurdan fluorescence with log-normal multipeak analysis

Naomi Hamada a and Marjorie L. Longo \*a

<sup>a</sup> Department of Chemical Engineering, University of California Davis, Davis, California 95616, United States

\*Corresponding authors: e-mail address: mllongo@ucdavis.edu

# **Abstract**

Phase separation phenomena in hybrid lipid/block copolymer/cholesterol bilayers combining polybutadiene-block-polyethylene oxide (PBdPEO), egg sphingomyelin (egg SM), and cholesterol were studied with fluorescence spectroscopy and microscopy for comparison to lipid bilayers composed of palmitoyl oleoyl phosphatidylcholine (POPC), egg SM, and cholesterol. Laurdan emission spectra were decomposed into three lognormal curves. The temperature dependence of the ratios of the areas of the middle and lowest energy peaks revealed temperature break-point (T<sub>break</sub>) values that were in better agreement, compared to generalized polarization inflection temperatures, with phase transition temperatures in giant unilamellar vesicles (GUVs). Agreement between GUV and spectroscopy results was further improved for hybrid vesicles by using the ratio of the area of the middle peak to the sum of the areas all three peaks to find the T<sub>break</sub> values. For the hybrid vesicles, trends at T<sub>break</sub> are hypothesized to be correlated with the mechanisms by which the phase transition takes place, supported by the compositional range as well as the morphologies of domains observed in GUVs. Low miscibility of PBdPEO and egg SM is suggested by the finding of relatively high T<sub>break</sub> values at cholesterol contents greater than 30 mol%. Further, GUV phase behavior suggests stronger partitioning of cholesterol into PBdPEO than into POPC, and less miscibility of PBdPEO than POPC with egg SM. These results, summarized using a heat-map, contribute to the limited body of knowledge regarding the effect of cholesterol on hybrid membranes, with potential application toward the development of such materials for drug delivery or membrane protein reconstitution.

Keywords: hybrid vesicles; membrane phase behavior; liquid-ordered; copolymer; fluorescence spectroscopy; multipeak analysis

# 1. Introduction

Hybrid membranes combining lipids and amphiphilic block copolymers have been a recent area of scientific interest, especially because of their potential value toward biomedical applications. Both lipid membranes and block copolymer membranes individually offer unique advantages, motivating the study of hybrid membranes. While the biocompatibility of lipid membranes has facilitated their usage in the areas of liposomal drug delivery and membrane protein reconstitution, the wide range of chemical functionality and increased mechanical stability of block copolymer membranes are also desirable [1]. Such hybrid membranes are thus appealing because they combine the favorable properties of both lipid and block copolymer membranes. In comparison to lipid-only or polymer-only membranes, hybrid membranes have been demonstrated to extend the functional lifetime of an incorporated membrane protein [2] and to increase the yield of cell-free expression of a membrane protein [3]. Hybridization of polymer vesicles with lipids has also been demonstrated to increase the efficacy of targeted vesicle binding to tumors in mice [4].

To further inform the application of hybrid membranes, it is important to understand their phase behavior, as this may have implications toward their function. For example, in lipid vesicles the formation of domains enriched in a cationic lipid has been suggested to enhance intracellular delivery of macromolecules [5,6]. The phase behavior of lipid membranes has been studied extensively. It is well documented that in the presence of cholesterol, certain lipid mixtures can display solid/fluid or fluid/fluid phase separation depending upon the mixture composition [7–9]. Similarly, phase separation in hybrid membranes has been reported for a variety of compositions [1,10]. However, the effect of cholesterol on the phase behavior of block copolymer and hybrid membranes has been explored to only a limited extent [10,11]. There thus exists a need for continued investigation of the phase behavior of hybrid membranes.

Fluorescent probes, including diphenylhexatriene (DPH) [12] and laurdan [13], have been used to study the phase behavior of both lipid-only [12–15] and hybrid membranes [16,17]. For this work, laurdan was chosen due to its greater sensitivity to the phase behavior of hybrid dipalmitoylphosphatidylcholine (DPPC)/polybutadiene-block-polyethylene oxide (PBdPEO) vesicles which we demonstrated in recent work [16]. Laurdan displays a red shift in its emission spectrum as the polarity of its local environment increases [13]. This is directly related to the hydration of the membrane, which is in turn dependent on the extent of the ordering of the membrane. The relative membrane polarity indicated by laurdan is quantified by calculation of generalized polarization (GP) values. Trends in laurdan GP values thus provide information regarding the phase behavior of the membrane [13]. To gain further insight into the phase behavior of lipid membranes, decomposition of laurdan emission spectra into multiple peaks has been proposed as an additional tool [18–20]. For the case of cholesterol-containing lipid membranes in particular, multipeak analysis has been proposed to provide greater insight into phase behavior than calculation of GP values [18]. Because the emission wavelength of laurdan depends strongly

on the polarity of the membrane, trends observed in the relative areas of the peaks returned by such decomposition approaches have been reported to correspond with the phase behavior of the membrane [18,19].

Here, we apply multipeak analysis to laurdan emission spectra, taken at sequential temperatures, of 3-component vesicles composed of the block copolymer PBdPEO or the lipid palmitoyl oleoyl phosphatidylcholine (POPC), egg sphingomyelin (egg SM), and cholesterol. This technique has not been used with hybrid membranes before, to the best of our knowledge, but presents a means of studying their phase behavior in greater depth than possible with the more general information provided by trends in laurdan GP values. A PBdPEO block copolymer with an average molecular weight of 950 g/mol, expected to form a relatively fluid membrane at room temperature [21], was used. Vesicles combining either POPC (solid-fluid transition temperature of -2 °C) or PBdPEO (glass transition temperature of ~-22 °C) and egg SM (solid-fluid transition temperature of ~39 °C [7]) are first compared as POPC and PBdPEO are expected to be fluid and egg SM is expected to be solid at room temperature. Then, analysis of laurdan emission spectra for lipid-only vesicles containing POPC, egg SM, and cholesterol is presented for a limited range of compositions. Subsequently for a broad range of compositions, laurdan emission spectra for hybrid vesicles containing PBdPEO, egg SM, and cholesterol is presented. For both hybrid and lipid-only vesicles with cholesterol, the phase behavior indicated by multipeak analysis is found to be in better agreement with fluorescence microscopy results in giant unilamellar vesicles (GUVs) than that indicated by laurdan GP values. Similar to the phase behavior reported for lipid-only vesicles [7], both solid/fluid and fluid/fluid phase separation are observed for hybrid GUVs containing cholesterol. Overall, our results suggest stronger partitioning of cholesterol into the copolymer PBdPEO than into POPC, and less miscibility of PBdPEO with egg SM in comparison to POPC and egg SM.

#### 2. Materials and Methods

#### 2.1 Materials

Egg sphingomyelin (egg SM), palmitoyl oleoyl phosphatidylcholine (POPC), egg lissamine rhodamine B phosphatidylethanolamine (egg rhod PE), and cholesterol were purchased from Avanti Polar Lipids, Inc. The diblock copolymer poly(1,2-butadiene)-*block*-poly(ethylene oxide) (PBdPEO), with an average molecular weight of 950 g/mol, (P41807C-BdEO, Bd(600)-*b*-EO(350), PDI = 1.06) was purchased from Polymer Source, Inc. 6-dodecanoyl-2-dimethylaminonaphthalene (laurdan) was purchased from AdipoGen Life Sciences. Texas Red 1,2-dihexadecanoyl-sn-glycero-3-phosphoethanolamine (Texas Red DHPE) was purchased from Biotium. All water used for experiments was purified with a Barnstead Nanopure System (Barnstead Thermolyne) and had a resistivity ≥17.8 MΩ·cm.

# 2.2 Preparation of large unilamellar vesicles (LUVs)

Appropriate volumes of lipid, polymer, and cholesterol stock solutions in chloroform and laurdan stock solution in ethanol were combined in clean glass vials. A gentle stream of nitrogen was used to evaporate the solvent, leaving a uniform film. To remove any residual solvent, the vials were then kept under vacuum for 2-24 hours. The dried film was heated in a water bath of at least 50 °C and rehydrated with water to a final lipid/polymer concentration of 2 mM. This solution was then passed 11 times through a polycarbonate membrane with 0.1 μm pores using a mini extruder (Avanti).

# 2.3 Preparation of giant unilamellar vesicles (GUVs)

Appropriate volumes of lipid, polymer, and cholesterol stock solutions in chloroform were combined in a clean glass vial and further diluted with chloroform to yield a final lipid/polymer concentration of 0.5 mg/mL. 0.2 mol% of egg rhodamine PE was incorporated into lipid-only giant unilamellar vesicles (GUVs); the same concentration of Texas Red DHPE was used instead for hybrid GUVs. The mole percentage of the lower melting temperature component (POPC or PBdPEO) was reduced in compensation. GUVs were prepared in a custom built electroformation chamber consisting of parallel platinum electrodes in a polytetrafluoroethylene housing. 25 µL of the prepared stock solution was spread over each electrode with a gastight Hamilton glass syringe, and a gentle stream of nitrogen was used to dry the electrodes. The chamber was then placed under vacuum for 2-24 hours to remove any residual solvent. Immediately prior to vesicle formation, glass coverslips were fixed over the openings of the chamber with vacuum grease and the sealed chamber was filled with water. The chamber temperature was maintained at 45 °C (lipid-only GUVs) or 50 °C (hybrid GUVs) with an external heating element. A sinusoidal wave with an amplitude of 3 V was applied at a frequency of 10 Hz for 30 minutes; then, the frequency was reduced to 3 Hz for 15 minutes. After this, 2 V/1 Hz were applied for 7.5 minutes, and then 2 V/0.5 Hz for 7.5 minutes. Prior to collection of GUVs, the chamber was allowed to cool freely to room temperature, typically requiring roughly 90 minutes. GUVs were stored in a plastic conical tube and imaged the same day.

To prepare a sample for imaging, a small aliquot of GUV suspension was added to a chamber formed by a glass slide, vacuum grease, and no. 1.5 cover slip. Images were collected using a Nikon Eclipse 80i equipped with either a 60x oil immersion or 60x air objective. The air objective was used for all images collected above or below room temperature to avoid thermal coupling of the sample and objective. A heated microscope stage (BoliOptics) was used to control the sample temperature. Sample temperatures were recorded as the average of the temperatures at the upper surfaces of the cover slip and glass slide, as measured by two resistance temperature detectors (Minco). To assess transition temperatures, GUVs were heated to 5-10 °C above the expected transition temperature, then cooled in increments of 2 °C while far from the expected transition

temperature. The temperature was then reduced in increments of 1 °C as the expected transition temperature was approached. Lipid-only GUVs were allowed to equilibrate for a minimum of 7 minutes at each temperature, while hybrid GUVs were allowed at least 10 minutes. The transition temperature was identified as the temperature at which domains first appeared upon cooling. Experimental uncertainty in T<sub>m</sub> was determined to be roughly a range of 1.5 °C, based on repeated experiments with selected compositions of GUVs.

### 2.4 Collection and analysis of laurdan emission spectra

LUVs containing laurdan were prepared as described above, using a lipid:probe ratio of 200:1. The prepared LUVs were diluted with water to a final lipid concentration of 200 µM immediately prior to fluorescence spectroscopy experiments. Laurdan emission spectra were collected from 370-600 nm with a Jasco spectrofluorometer using an excitation wavelength of 355 nm. Samples were heated to the highest temperature of interest, allowed to equilibrate for 30 minutes, then cooled in increments of 2 °C with an incubation time of 3 minutes at each temperature. Each sample was subjected to only one heating/cooling cycle prior to being discarded.

Laurdan generalized polarization (GP) provides insight into membrane polarity, with higher GP values corresponding to a more polar membrane. GP values were calculated using Equation (1), where  $I_{440}$  and  $I_{490}$  are the respective intensities of the laurdan emission spectrum at 440 nm and 490 nm.

$$GP = \frac{I_{440} - I_{490}}{I_{440} + I_{490}} \tag{1}$$

Least squares regression was also applied to fit a sigmoidal equation to calculated GP values (Equation (2)) [18].  $GP_{max}$  and  $GP_{min}$  represent the upper and lower limits of the GP curve, while n is a fitting parameter related to the slope of the curve in the vicinity of  $T_{mid}$ .  $T_{mid}$  represents the inflection point of the curve. Uncertainty values for  $T_{mid}$  were expressed as the standard deviation error for the fitting of this parameter.

$$GP(T) = \frac{GP_{max} - GP_{min}}{1 + e^{(T - T_{mid})n}} + GP_{min}$$
(2)

Decomposition of laurdan emission spectra into multiple peaks was also carried out to gain further insight into membrane phase behavior. Emission spectra were fit in Python with the sum of multiple lognormal curves using least squares regression as described in Puff et al. [18], with each lognormal curve characterized by an equation of the following form:

$$y = A_0 + A_1 exp \left[ -\left(\frac{\ln\left(\frac{x}{A_2}\right)}{A_3}\right)^2 \right]$$
 (3)

 $A_0$  represents the baseline,  $A_1$  the amplitude,  $A_2$  the position, and  $A_3$  the width of the fitted curve. All parameters besides  $A_0$  were constrained to be greater than 0 when performing the fit. Additionally, the peak position  $A_2$  was constrained to the range of measured wavelengths, which spans the observed emission spectrum of laurdan in the membrane. Prior to spectral decomposition, emission intensities were expressed as a function of energy at each wavelength using the relationship  $(h^*c/E^2)$ , where h is Planck's constant, c is the speed of light in a vacuum, and E is the energy corresponding to each wavelength (calculated as  $h^*c/\lambda$ , where  $\lambda$  is the wavelength) [18,22,23].

When three-peak fits to laurdan emission spectra were used, peak area ratios were calculated at each temperature studied as the area of the middle energy peak divided by the area of the lowest energy peak unless otherwise specified. Peak area ratio plots were fit with a three-piece linear function in Python to identify the temperature at which the first two lines met, which is expected to be within the range the phase transition temperature of the membrane, as described in Puff et al [18]. Uncertainty values for this position were reported as the standard deviation error in the intersection of these lines as calculated from the standard deviation error of the piecewise linear fit applied to each peak area ratio plot.

### 3. Results and Discussion

A combination of fluorescence spectroscopy and microscopy was used to study phase behavior in large unilamellar vesicles (LUVs) and giant unilamellar vesicles (GUVs) composed of palmitoyl oleoyl phosphatidylcholine (POPC) or polybutadiene-*block*-polyethylene oxide (PBdPEO), egg sphingomyelin (egg SM), and cholesterol. Compositions are reported as mole percentages.

#### 3.1 Cholesterol-free vesicles

First, a selected 40-60 mol% composition of POPC-egg SM and PBdPEO-egg SM LUVs was compared. Calculating the generalized polarization (GP) of laurdan in these LUVs as described in Equation (1)yielded the plot in Figure 1A. Both curves display a sigmoidal dependence of GP on temperature, with the inflection point ( $T_{mid}$ ) of each curve representing the approximate midpoint temperature for the formation of solid phase domains [24]. For the POPC-egg SM LUVs, laurdan GP indicated a  $T_{mid}$  of 27.5±0.2 °C. For the PBdPEO-egg SM LUVs,  $T_{mid}$  was 33.9±0.2 °C. Figure 1B shows fluorescence images of 40-60 mol% POPC-egg SM and PBdPEO-egg SM GUVs. After heating GUVs so that a single phase was observed, dark domains formed upon cooling. The

temperature at which domains first appeared upon cooling  $(T_m)$ , 32.0±1.5 °C for POPC-egg SM and 33.0±1.5 °C for PBdPEO-egg SM, was within a few degrees of  $T_{mid}$  measured by laurdan GP. In both cases, irregularly shaped domains were observed as shown in Figure 1B, indicative of solid/fluid phase separation.

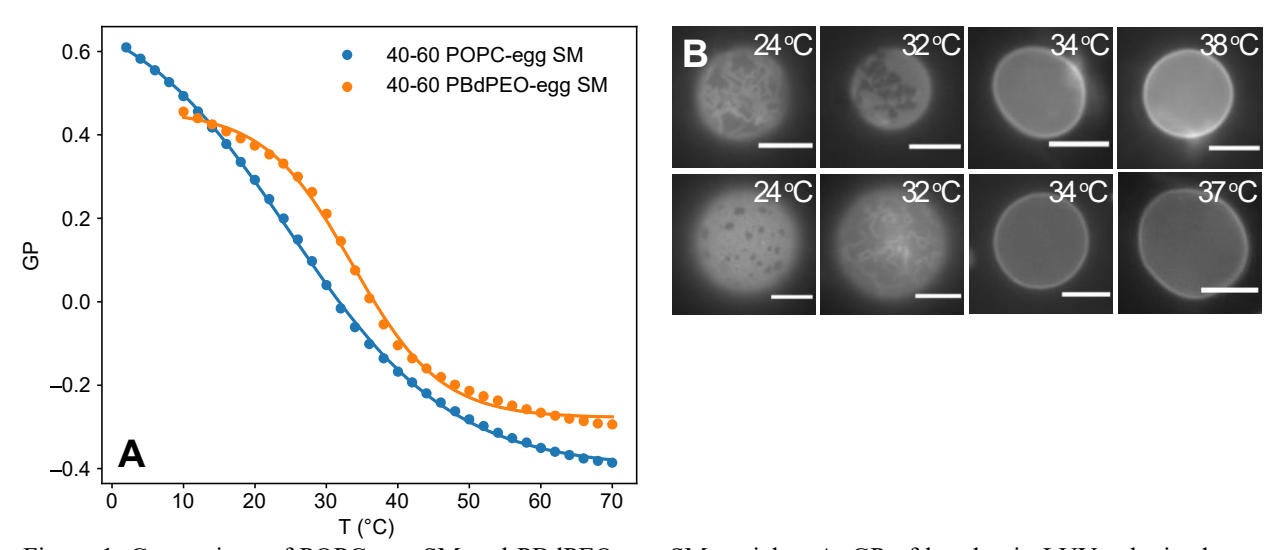


Figure 1. Comparison of POPC-egg SM and PBdPEO-egg SM vesicles. A. GP of laurdan in LUVs obtained upon cooling. The inflection point,  $T_{mid}$ , for the POPC-egg SM LUVs is  $27.5 \pm 0.2$  °C, and for the PBdPEO-egg SM LUVs is  $33.9 \pm 0.2$  °C. Plotted points show calculated GP values, while lines show a fit to Equation (2). B. Fluorescence microscopy of GUVs. Top row, 40-60 mol% POPC-egg SM GUVs; bottom row, 40-60 mol% PBdPEO-egg SM. The temperature at which domains in GUV populations first appeared upon cooling,  $T_{m}$ , is  $32.0 \pm 1.5$  °C for the POPC-egg SM GUVs and  $33.0 \pm 1.5$  °C for the PBdPEO-egg SM GUVs. Scale bar is  $10 \ \mu m$ .

### 3.2 Analysis of laurdan spectroscopy results for POPC-egg SM-cholesterol LUVs

These methods were then applied to POPC-egg SM-cholesterol vesicles containing sufficient cholesterol to promote liquid/liquid phase separation. Laurdan GP values in POPC-egg SM-cholesterol LUVs are shown in Figure 2A. The shapes of the GP curves are generally sigmoidal, suggesting a phase transition takes place within the temperature range studied. However, the shallow slopes of the GP curves contrast especially with the results shown in Figure 1A for vesicles containing no cholesterol, for which a less broad phase transition is expected. This can make clear assessment of the inflection point difficult. For egg phosphatidylcholine-egg SM-cholesterol LUVs containing less cholesterol, good agreement between GP analysis and GUV phase transitions has been reported [18]. However, for the POPC-egg SM-cholesterol compositions shown in Figure 2A, the T<sub>mid</sub> values indicated by laurdan GP range from roughly 40-50 °C. These temperatures are significantly above the range of 20-35 °C expected for miscibility of the two liquid phases for similar vesicle compositions [9,18].

Decomposition of laurdan emission spectra into multiple peaks [18] was therefore carried out in an attempt to gain further insight into the phase behavior of cholesterol-containing membranes beyond the information provided by GP values. Three lognormal peaks characterized by Equation (3) were used to fit laurdan emission spectra as described in Puff et al [18]. An example of such a decomposition for 30-40-30 mol% POPC-egg SM-chol at 20 °C is shown in Figure S1.

For the three-peak fits of laurdan emission spectra in POPC-egg SM-cholesterol vesicles, the peak positions typically ranged from ~2.89-2.92 eV (425-430 nm, high-eV peak), ~2.67-2.79 eV (445-465 nm, mid-eV peak), and ~2.48-2.58 eV (480-500 nm, low-eV peak) across the range of temperatures studied. This is comparable to the ranges reported for similar multipeak analyses of laurdan [18,25] and BADAN [26], a probe with the same fluorescent moiety as laurdan. These peaks are hypothesized to respectively correspond to a non-hydrogen bonded state, an immobilized hydrogen bonded state, and a mobile hydrogen bonded state [26]. The ratio of the areas of the mideV peak and low-eV peak has thus been proposed as a metric of the relative amount of the liquid ordered phase in cholesterol-containing vesicles [18].

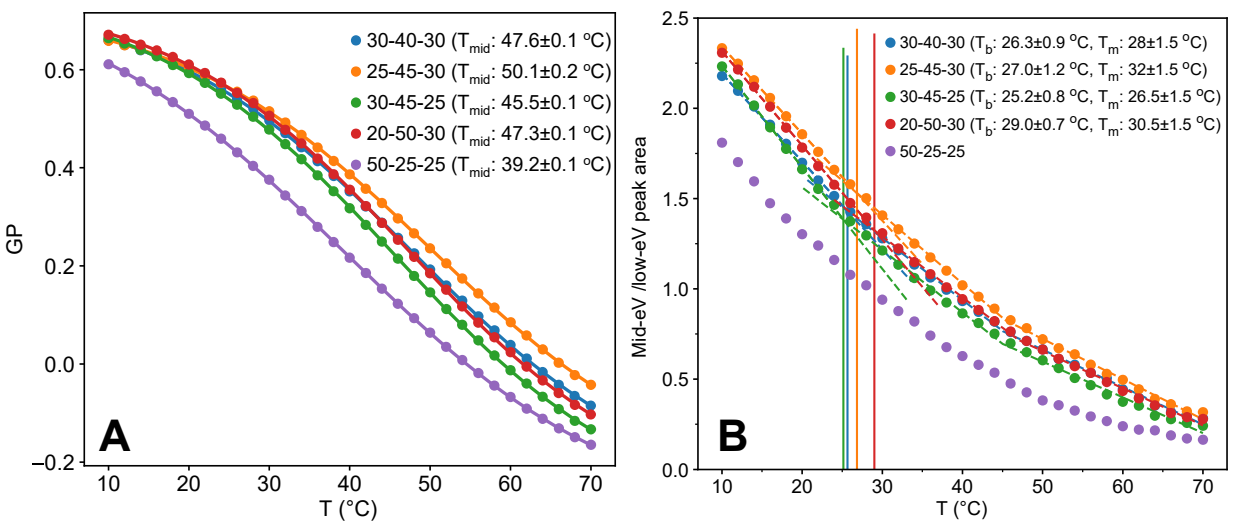


Figure 2. A. GP of laurdan in POPC-egg SM-cholesterol LUVs of the specified mole percentages. Lines represent fits to an equation for a sigmoidal curve, as described in Equation (2), and  $T_{mid}$  is the inflection point of this fit. B. Plot of the ratios of the mid-eV and low-eV peak areas resulting from the decomposition of laurdan emission spectrum into three peaks. Dashed lines indicate the piecewise linear function used to evaluate  $T_{break}$ . Vertical lines indicate  $T_{break}$ , the temperature at which the slope of the plot changes ( $T_b$  in the legend).  $T_m$  in the legend refers to the temperature at which domains first appeared upon cooling indicated by fluorescence microscopy images of GUVs.

The results of carrying out three-peak laurdan emission spectra decomposition for POPC-egg SM-cholesterol LUVs are therefore plotted in Figure 2B as the area of the mid-eV peak divided by the area of the low-eV peak [18]. As described in Puff et al. [18], this resulted in concave plots. A three-piece linear fit was applied to each plot, and the temperatures at which the first line and second line meet (T<sub>break</sub>, indicated by the vertical lines in Figure 2B) lie within the range of the miscibility transition expected based on previous literature [9,18]. Moreover, plotting these transitions as a heat map in Figure S2 on a 3-component triangle yielded expected trends [9]. Therefore, multipeak analysis may be a more accurate approach than GP analysis to interpreting this laurdan spectral data.

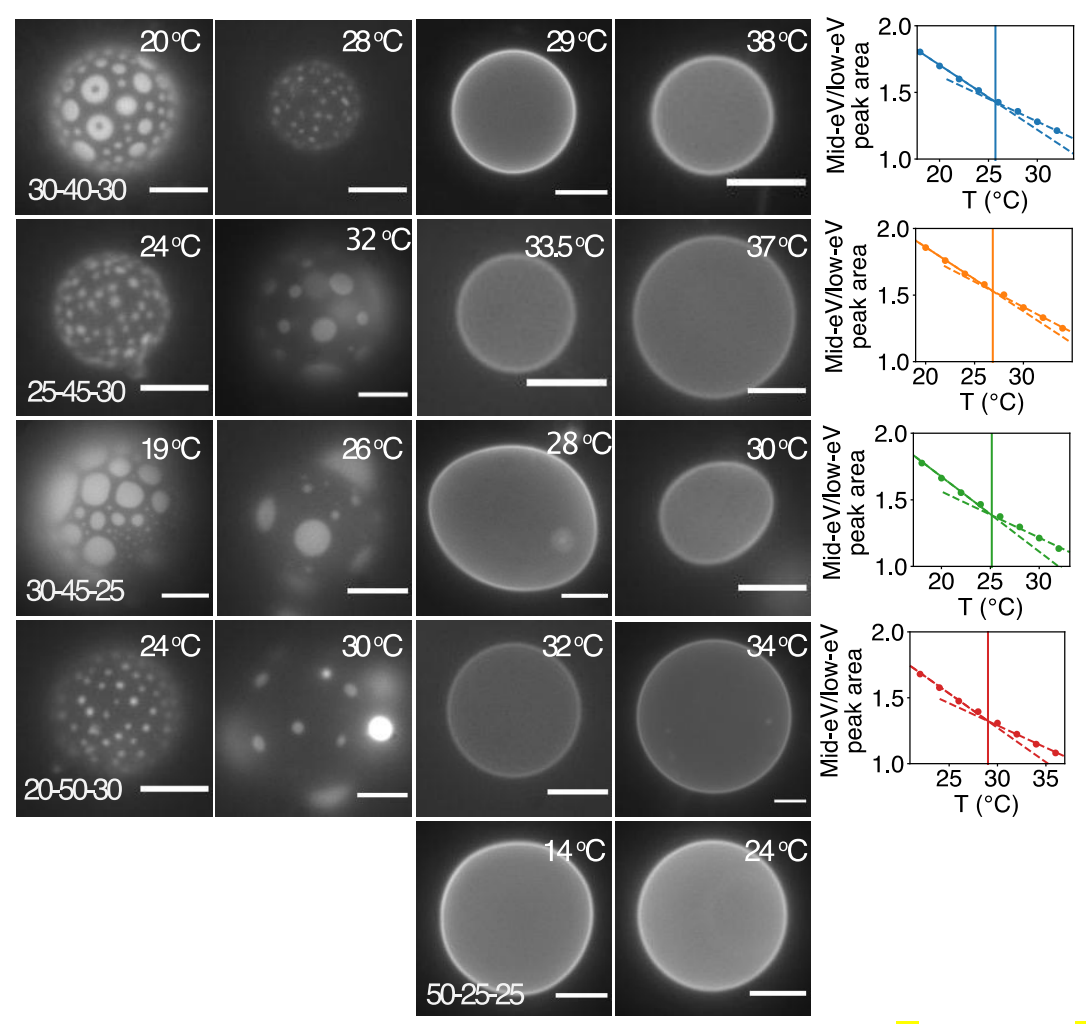


Figure 3. Fluorescence microscopy images of POPC-egg SM-cholesterol GUVs of the specified mole percentages across a range of temperatures. Some deformation of GUVs is evident at higher temperatures, likely due to a combination of the increased fluidity of the membrane and convection within the sample volume. Scale bar represents 10 μm. Rightmost panels show portions of Figure 2B for individual compositions in the vicinity of T<sub>break</sub>. Dashed lines indicate the piecewise linear function used to evaluate T<sub>break</sub>. Vertical line denotes T<sub>break</sub>

# 3.3 POPC-egg SM-cholesterol GUV behavior

For comparison, GUVs of the same compositions were examined, as shown in Figure 3. The temperatures at which domains first appeared upon cooling (T<sub>m</sub>) were in good agreement with T<sub>break</sub> (see plots in Figure 3, and Table S1) but not T<sub>mid</sub> laurdan GP results (see legends of Figure 2). T<sub>m</sub> values were also in good agreement with previously published work regarding GUVs composed of a similar lipid mixture (which instead incorporated palmitoyl sphingomyelin (PSM), the primary component of egg SM) [9]. GUVs typically displayed bright, round domains on a dark background, suggesting the presence of both the liquid disordered (POPC-rich) and liquid ordered (egg SM-rich) phases. For the 50-25-25 mol% POPC-egg SM-cholesterol GUVs, domains were

not observed at room temperature or at the lowest temperature accessible to us (~13 °C). This composition lies at the very edge of the previously reported two-phase region for POPC-PSM-cholesterol GUVs [9], so it is possible the slight compositional differences between egg SM and PSM may have resulted in the observation of only one phase for this composition.

# 3.4 Analysis of laurdan spectroscopy results for PBdPEO-egg SM-cholesterol LUVs

Given the consistent results of the three-peak decomposition for lipid-only membranes containing cholesterol (i.e., good agreement of T<sub>break</sub> with T<sub>m</sub>), we then applied the same approach to hybrid membranes containing the block copolymer polybutadiene-*block*-polyethylene oxide instead of POPC. Results of laurdan GP calculation and laurdan emission spectrum decomposition are shown in Figure 4. As for the POPC-egg SM-cholesterol vesicles, the shallow slopes of the laurdan GP curves suggest a broad phase transition. T<sub>mid</sub> values ranged from ~35-56 °C (legend of Figure 4A) by fitting to Equation (2), similar to those indicated by laurdan GP for POPC-egg SM-cholesterol LUVs.

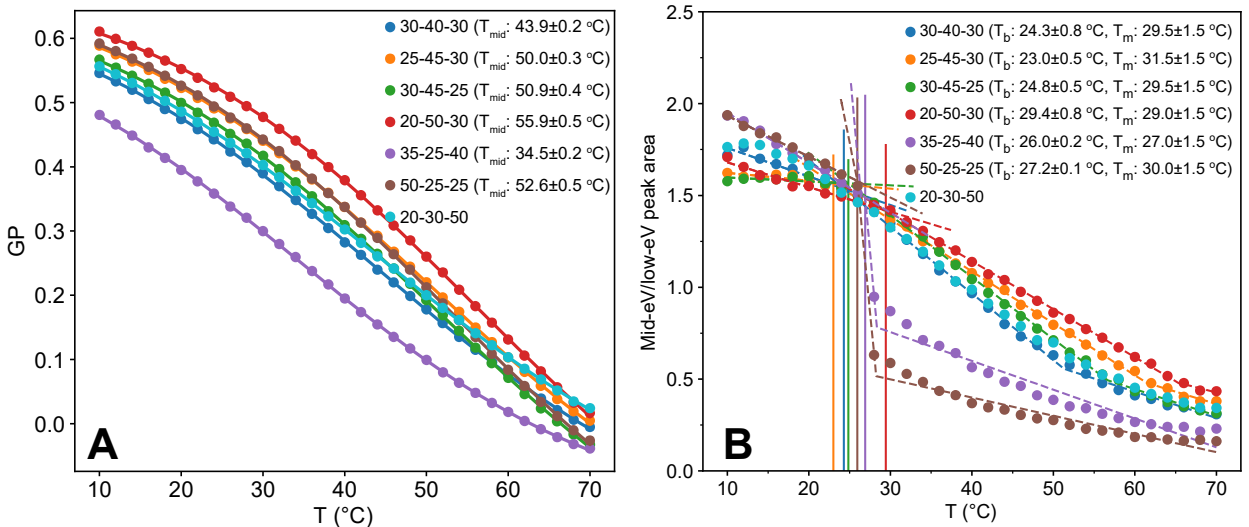


Figure 4. A. GP of laurdan in PBdPEO-egg SM-chol LUVs of the specified mole percentages. T<sub>mid</sub> is the inflection point indicated by fitting to Equation (2). B. Ratio of the areas beneath the mid-eV and low-eV peaks resulting from the decomposition into three curves of laurdan emission spectra in PBdPEO-egg SM-chol LUVs of the specified mole percentages. Vertical lines indicate the first change in slope at temperature T<sub>break</sub>. In the legend, T<sub>b</sub> refers to T<sub>break</sub>. T<sub>m</sub> in the legend refers to the temperature at which domains first appeared upon cooling indicated by fluorescence microscopy images of GUVs. Dashed lines indicate the piecewise linear function used to evaluate T<sub>break</sub>.

Figure S3 shows an example of a three-peak fit to a laurdan emission spectrum for 30-40-30 mol% PBdPEO-egg SM-chol at 20 °C. The small values of the residuals and relatively Gaussian distribution suggest a good fit is achieved with three peaks. A difference in the shapes of the peak area ratio profiles is clear between the hybrid (Figure 4B) and lipid-only (Figure 2B) membranes. While the lipid-only membranes had concave peak area ratio plots, those for the hybrid membranes appeared roughly sigmoidal, with some compositions displaying a discontinuity at T<sub>break</sub> and others

displaying a change in slope. Additionally, T<sub>break</sub> values were in a similar range, ~23-29 °C (legend of Figure 4B), to those indicated for POPC-egg SM-cholesterol LUVs.

To further investigate, peak area ratio plots were constructed for a broad range of compositions of hybrid LUVs (Figure 5). At T<sub>break</sub>, either a discontinuity (Figure 5A) or only a change in slope (Figure 5B) was observed depending on the composition. The peak area ratio is expected to correlate with the relative amount of the liquid ordered phase—more specifically, with the relative amount of hydrogen-bound but immobile laurdan [18,26]. This suggests that for the compositions plotted in Figure 5A, once the temperature decreases below T<sub>break</sub>, the liquid-ordered lipid population increases sharply. For the compositions in Figure 5B, after the temperature decreases below T<sub>break</sub>, the size of this population increases gradually.

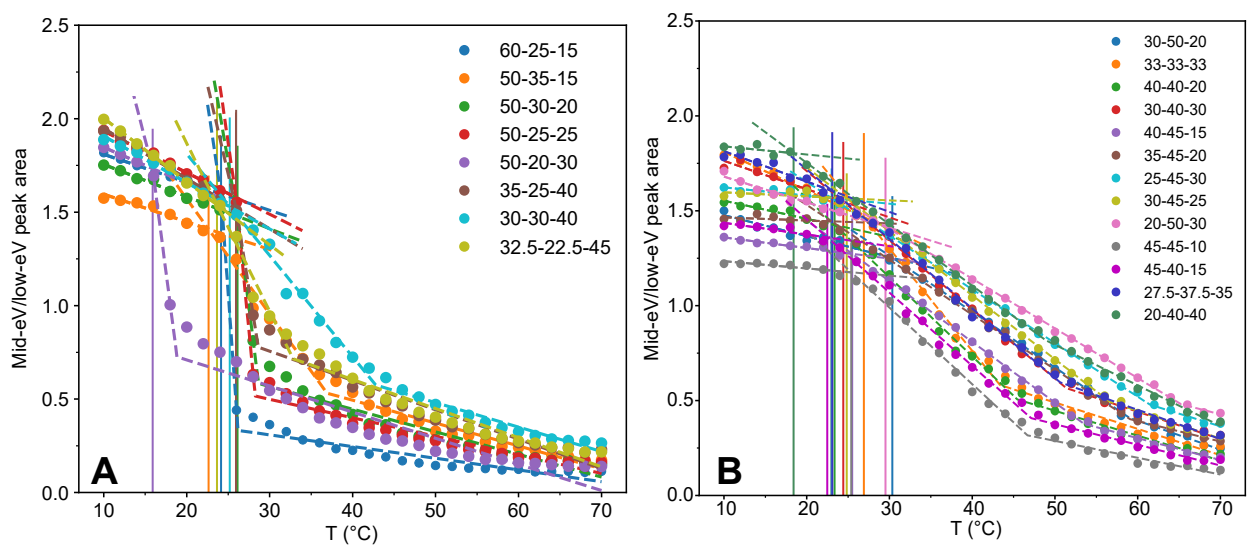


Figure 5. Comparison of trends in the temperature dependence of the peak area ratio plots for PBdPEO-egg SM-chol LUVs of the specified mole percentages. Dashed lines indicate the piecewise linear function used to evaluate  $T_{break}$ . A. Compositions for which the peak area ratio plot shows a discontinuity at  $T_{break}$ . B. Compositions for which the peak area ratio plot shows only a change in slope at  $T_{break}$ .

To better visualize any compositional trends in T<sub>break</sub> and in the peak area ratio plots for hybrid LUVs, a 3-component triangle (Figure 6A) was used. T<sub>break</sub> values are plotted as a heat map on the 3-component triangle. In Figure 6A, red circles indicate compositions displaying a discontinuity in their peak area ratio plot. This is not a phase diagram, as the results are not shown at a single temperature, but instead represents an overview of the data presented above. For comparison, a similar figure was constructed for the POPC-egg SM-cholesterol LUVs discussed above (Figure S2).

The  $T_{break}$  values shown on the heat maps in Figure 6 tend to increase as the amount of egg SM is increased and the amount of cholesterol is decreased, similar to the trends reported for lipid vesicles [9]. The range of temperatures observed for  $T_{break}$  (~15-30 °C for the compositions studied here) is also similar to the miscibility transitions reported in POPC-PSM-cholesterol GUVs of

comparable compositions [9]. For the hybrid vesicles, however, T<sub>break</sub> is significantly higher at high cholesterol contents (>30%) indicating relatively less miscibility between PBdPEO and egg SM. In this respect, some similarity is shared with the phase coexistence region of dioleoylphosphatidylcholine (DOPC)-PSM-cholesterol vesicles, which displays miscibility temperature values near room temperature at ~40 mol% cholesterol [9].

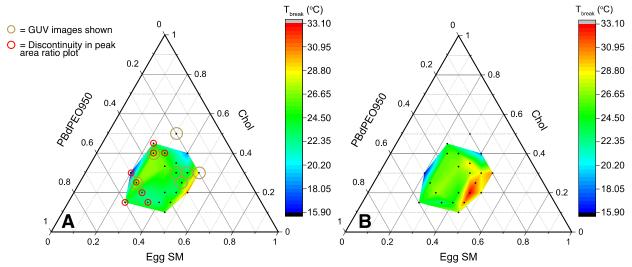


Figure 6. Heat maps of T<sub>break</sub> values indicated by laurdan in PBdPEO-egg SM-cholesterol LUVs. A. T<sub>break</sub> values calculated from the ratio of the mid-eV and low-eV peak areas. Gold circles mark compositions for which images of GUVs are shown. Compositions for which a discontinuity is observed in the laurdan peak area ratio plots are indicated with a red circle. For the single point plotted outside the edges of the heat map, only a single phase was observed for GUVs at the lowest accessible temperature (~13 °C). However, the edges of the heat map do not indicate the boundaries of a phase coexistence region. B. T<sub>break</sub> values recalculated based on the ratio of the mid-eV peak area to the sum of the areas of all three peaks. T<sub>break</sub> was obtained from the meeting point of the first and second lines of a piecewise linear fit to the peak area ratios, as in part A.

For two-phase lipid GUVs, phase separation by spinodal decomposition has been reported for compositions with the average area fraction of one phase ranging from 0.3-0.7 (i.e., similar proportions of each phase) [27]. Outside of this range, phase separation is initiated by nucleation and growth, which takes place when there is a discontinuity in the composition associated with the new phase. Therefore, it is not too surprising that the compositions for which a discontinuity in the peak area ratio plot was observed are all positioned roughly on the left side of the phase space explored, which is perhaps in the compositional range for nucleation and growth. The lack of discontinuities in the peak area ratio plots for the remainder of the compositions suggests that they phase separate by spinodal composition, which may be visible somewhat in the domain morphologies observed in GUVs.

### 3.5 PBdPEO-egg SM-cholesterol GUVs and further analysis of laurdan spectroscopy results

For comparison, GUVs of compositions from Figure 4 were imaged. The temperatures at which domains first appeared upon cooling  $(T_m)$  were in better agreement with  $T_{break}$  than with the  $T_{mid}$  laurdan results (see legends of Figure 4). To attempt to gain better agreement between  $T_{break}$  and

 $T_m$ , an additional fitting approach was used. The relative amount of the mid-eV peak, reported to be correlated with the relative abundance of the liquid ordered phase [18], was recalculated by comparing the area of the mid-eV peak to the area of all three peaks (Table S2). Interestingly, this resulted in better agreement for the compositions with larger ( $\sim$ >4-5 °C) discrepancies between  $T_{break}$  and  $T_m$ . For the compositions for which there was little difference between  $T_{break}$  and  $T_m$ , this recalculation did not significantly change  $T_{break}$  (typically less than a  $\sim$ 1 °C difference after recalculation).

For the hybrid membranes, certain compositions displayed a high-eV peak area that remained relatively consistent at all temperatures studied, both above and below T<sub>m</sub> in GUVs. In comparison, for the lipid-only vesicles in this work the area beneath the high-eV peak increased and the area beneath the low-eV peak decreased as the temperature decreased (Figure S4), consistent with the expectation of an increasingly ordered membrane at lower temperatures and with previously reported results [18,19]. DOPC vesicles [19] also unexpectedly displayed high energy peaks of relatively constant area with temperature in another work. The authors attributed the relatively constant area of these peaks to the presence of an energetically unfavorable but still observable population of non-hydrogen bonded laurdan molecules at high temperature, based on their report of a short lifetime at this wavelength. It is possible that such a phenomenon is taking place in the hybrid membranes as well. In such a case, considering the recalculation of the peak area ratios as described above may provide more accurate insight into the phase transition temperatures of hybrid vesicles.

Recalculating peak area ratios as the area of the mid-eV peak divided by the sum of the areas of the high-eV, mid-eV, and low-eV peaks and evaluating  $T_{break}$  resulted in the heat map shown in Figure 6B. Similar trends are observed for vesicles containing lower amounts of egg SM as shown in Figure 6A. However, for vesicles incorporating more than ~40% egg SM, recalculated  $T_{break}$  values were ~5-7 °C higher, which is more consistent with the trends observed for  $T_m$  in GUVs.

It should also be noted that below T<sub>m</sub>, it was typically more common to observe bright, single phase GUVs when PBdPEO rather than POPC was incorporated. This may be due to budding away of the dark phase prior to imaging; significant and rapid budding has been previously reported in hybrid GUVs incorporating a different triblock copolymer [28]. Therefore, discrepancies in T<sub>m</sub> and T<sub>break</sub> may also occur from differences in composition of hybrid GUVs and LUVs respectively attributed to rapid budding before the heating and cooling cycle. Alternatively, such compositional variations could arise from incomplete detachment of GUVs immediately after formation but prior to cooling [29–31]. This would allow domain formation in the interconnected GUV buds prior to their separation and collection, resulting in subsequent compositional differences amongst individual GUVs.

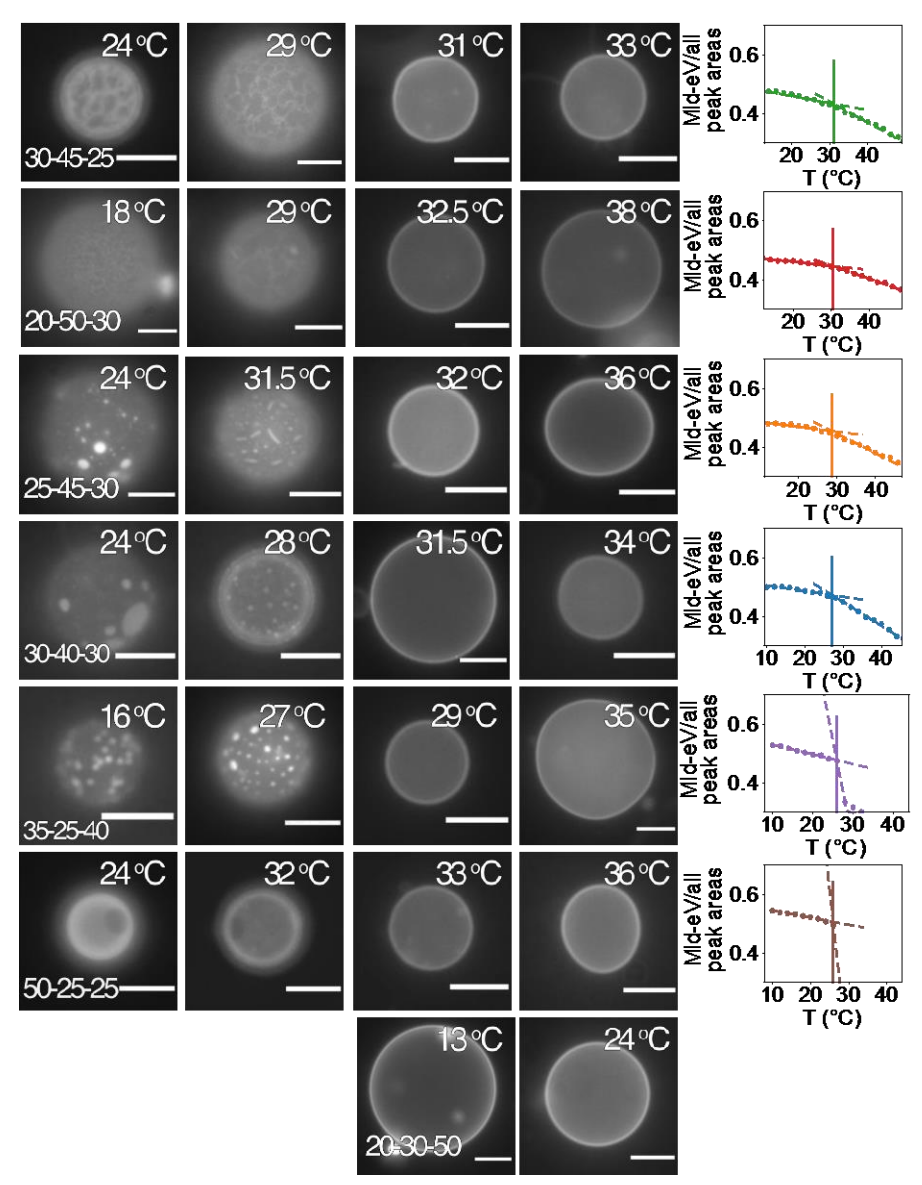


Figure 7. Fluorescence microscopy images of giant unilamellar vesicles consisting of PBdPEO-egg SM-cholesterol at the specified mole percentages across a range of temperatures. For the vesicles containing 50 mol% cholesterol, domains were not observed even at the lowest accessible temperature. For the 50-25-25 mol% sample, T<sub>m</sub> was assessed by heating rather than cooling the vesicles, as excessive budding away of domains upon cooling complicated assessment of T<sub>m</sub>. Scale bar represents 10 μm. Rightmost panels show portions of peak area ratio plots recalculated by dividing the area of the mid-eV peak by the sum of the areas of all three peaks for individual compositions in the vicinity of T<sub>break</sub>. Dashed lines indicate the piecewise linear function used to evaluate T<sub>break</sub>. Vertical line denotes T<sub>break</sub>.

Fluorescence images of GUVs of compositions from Figure 4 are shown in Figure 7. The panels on the far right of Figure 7 show selected regions of mid eV/all eV peaks near the refitted T<sub>break</sub> values for each composition. The compositions in rows 3-6 of Figure 7 (25-45-30, 30-40-30, 35-25-40, and 50-25-25 mol% PBdPEO-egg SM-cholesterol) appear to display coexisting fluid phases, based on the presence of round domains. In this case, the dark phase is likely rich in egg SM, given that below T<sub>m</sub> this dark phase makes up the majority of the vesicle surface area for

compositions richer in egg SM and less of the surface area when less egg SM is included. Circular domains have been previously reported in hybrid membranes upon inclusion of cholesterol and were hypothesized to be a liquid ordered-like phase [10].

In contrast to POPC-egg SM-cholesterol GUVs of the same compositions (Figure 3), the GUVs in rows 1 and 2 of Figure 7 (30-45-25 and 20-50-30 mol% PBdPEO-egg SM-cholesterol) appear to display predominantly solid/fluid instead of fluid/fluid phase separation, based on the irregularity of the domain shapes. This indicates greater amounts of cholesterol may be required to induce fluid/fluid phase separation in hybrid membranes as compared to lipid membranes. This result suggests that cholesterol partitions to a greater extent into PBdPEO in comparison to fluid lipids such as POPC. Of note, for POPC-PSM-cholesterol compositions with greater amounts of PSM, a three-phase region consisting of solid, liquid ordered, and liquid disordered phases with an upper bound delineated by the observed transition from fluid/fluid to solid/fluid phase separation has been suggested to exist across a range of cholesterol concentrations (~10-25 mol%) [9]. It is possible that one or both of the compositions of the GUVs in rows 1 and 2 of Figure 7 may lie within such a three-phase region as well, with T<sub>break</sub> perhaps corresponding to the appearance of the liquid-ordered phase as the sample is cooled.

For the 20-30-50 mol% PBdPEO-egg SM-cholesterol GUVs, no phase separated vesicles were observed at 13 °C or above, consistent with the observation that greater amounts of cholesterol were required to induce fluid/fluid phase separation in hybrid membranes than in lipid-only membranes. For comparison, a phase diagram for POPC-PSM-cholesterol GUVs indicates a single fluid phase exists above ~35 mol % cholesterol at temperatures greater than 15 °C [9]. Similarly, while 50-25-25 mol% PBdPEO-egg SM-cholesterol GUVs displayed dark, round domains up to ~32 °C, phase separation was not observed for POPC-egg SM-cholesterol GUVs of the same composition at or above ~13 °C, the lowest accessible temperature (Figure 3).

Rows 2-3 of Figure 7 (20-50-30 and 25-45-30 mol% PBdPEO-egg SM-cholesterol) show hybrid GUVs that displayed domain morphologies suggestive of spinodal decomposition below T<sub>m</sub>. For the 20-50-30 mol% GUVs, at low temperatures the widespread, grainy appearance of the domains and the low contrast between light and dark phases resemble the early stages of spinodal decomposition. Similarly, for the 25-45-30 mol% PBdPEO-egg SM-cholesterol GUVs elongation of domains is observed just below T<sub>m</sub>. Such morphologies have been observed in GUVs undergoing spinodal decomposition [7,32] and are attributed to reduced line tension near a critical point [7]. Additionally, these GUVs as well as those in rows 1 and 4 of Figure 7 (30-45-25 and 30-40-30 mol% PBdPEO-egg SM-cholesterol) display relatively low contrast in the brightness of light and dark domains—especially just below T<sub>m</sub>. This is indicative of a gradual change in composition, and thus weak partitioning of the probe. In agreement with these observations, these mixtures fall within the compositional region that was hypothesized to phase separate by gradual spinodal decomposition based upon laurdan multipeak analysis.

Of note, the length scales of the domains observed in GUVs and in LUVs are inherently different. Fluorescence microscopy enables observation of micron-scale domains in GUVs. While there may be temperatures at which stable nanodomains exist in GUVs but for some reason do not coalesce, this phenomenon occurs at a length scale unresolvable by fluorescence microscopy. LUVs, however, have diameters of ~100 nm; any domains that form in LUVs accordingly have sizes on the order of 100 nm or less. The laurdan experiments performed with LUVs would therefore detect the formation of such nanoscale domains. Theoretically, the same laurdan experiments could be carried out using GUVs, although our preliminary attempts to do so were limited by the low concentration of GUVs in solution yielded by electroformation. Further optimization of such experiments could allow for comparison between spectroscopy and microscopy results in GUVs.

To gauge the possible usefulness of multipeak analysis applied to cholesterol-free membranes, T<sub>break</sub> was evaluated for 40-60 mol% PBdPEO-egg SM vesicles based on the ratio of areas of the mid-eV peaks to the sum of the areas of all three peaks (Figure S5). A discontinuity in the vicinity of T<sub>break</sub> was observed, suggesting a significant difference in the compositions of the solid and fluid phases at T<sub>break</sub>. T<sub>break</sub> was 29.6±0.4 °C, less than both the GP T<sub>mid</sub> of 33.9±0.2 °C and the GUV T<sub>m</sub> of 33.0±1.5 °C. T<sub>break</sub> resulting from analysis of the ratios of the areas of the mid-eV and low-eV peaks for 40-60 mol% POPC-egg SM vesicles (Figure S5) was 36.7±0.8 °C, greater than both the GP T<sub>mid</sub> of 27.5±0.2 °C and the GUV T<sub>m</sub> of 32.0±1.5 °C. For POPC-egg SM LUVs, a gradual change in slope is observed in the vicinity of T<sub>break</sub>, similar to the trends observed for POPC-egg SM-cholesterol LUVs and suggestive of more gradual changes in the compositions of the two phases as the temperature is decreased. For cholesterol-free vesicles, which undergo a solid to fluid phase transition, laurdan GP analysis could potentially be used to more accurately determine the temperature at which solidification begins and the temperature at which half of the lipids have transitioned to the solid phase, as described in our previous work [16]. GUV T<sub>m</sub> values would then be expected to lie within the range of these temperatures. Conversely, multipeak analysis of laurdan emission spectra indicates a single temperature, T<sub>break</sub>. This may correspond more accurately to the behavior observed for GUVs in which the liquid ordered phase is present, typically resulting in domains that coalesce rapidly even just below T<sub>m</sub>.

#### 4. Conclusions

Fluorescence spectroscopy and microscopy were employed to study the phase behavior of POPC-egg SM-cholesterol and PBdPEO-egg SM-cholesterol vesicles. While laurdan GP indicated phase behavior consistent with observations of GUVs for POPC-egg SM and PBdPEO-egg SM vesicles, multipeak analysis of laurdan emission spectra was found to provide more accurate insight into phase behavior than analysis of laurdan GP values for cholesterol-containing lipid-only and hybrid vesicles. For hybrid vesicles, taking the ratio of the area of the middle energy peak to the sum of the areas of all peaks improved the temperature-dependent agreement with GUV behavior in

comparison to the ratio of the area of the middle peak to the area of the lowest energy peak. Either a more gradual change in slope or a discontinuity around the break-point of this ratio was observed for the hybrid vesicles. We hypothesize that these trends correspond to the mechanism by which phase separation proceeds (spinodal decomposition or nucleation and growth) based on the characteristic shapes of the peak area ratio plots, the compositions for which each profile was observed, and the morphologies of domains in GUVs of corresponding compositions. The relatively high T<sub>break</sub> values at cholesterol contents greater than 30 mol% are suggestive of low miscibility of PBdPEO and egg SM. Additionally, greater amounts of cholesterol were observed to be required to induce fluid/fluid phase separation in hybrid GUVs than in lipid-only GUVs. This suggests stronger partitioning of cholesterol into PBdPEO than into POPC. These results, which we summarized on a heat map, may inform the further investigation of the phase behavior of hybrid vesicles toward applications such as drug delivery.

## Acknowledgements

This material is based upon work supported by the National Science Foundation under Grant No. DMR – 1806366.

### Appendix A. Supplementary data

Supplementary data to this article can be found online.

#### **References:**

- [1] D. Chen, M.M. Santore, Hybrid copolymer–phospholipid vesicles: phase separation resembling mixed phospholipid lamellae, but with mechanical stability and control, Soft Matter. 11 (2015) 2617–2626. https://doi.org/10.1039/C4SM02502D.
- [2] S. Khan, M. Li, S.P. Muench, L.J.C. Jeuken, P.A. Beales, Durable proteo-hybrid vesicles for the extended functional lifetime of membrane proteins in bionanotechnology, Chem. Commun. 52 (2016) 11020–11023. https://doi.org/10.1039/C6CC04207D.
- [3] M.L. Jacobs, M.A. Boyd, N.P. Kamat, Diblock copolymers enhance folding of a mechanosensitive membrane protein during cell-free expression, PNAS. 116 (2019) 4031–4036. https://doi.org/10.1073/pnas.1814775116.
- [4] Z. Cheng, D.R. Elias, N.P. Kamat, E.D. Johnston, A. Poloukhtine, V. Popik, D.A. Hammer, A. Tsourkas, Improved Tumor Targeting of Polymer-Based Nanovesicles Using Polymer-Lipid Blends, Bioconjugate Chem. 22 (2011) 2021–2029. https://doi.org/10.1021/bc200214g.
- [5] Z.I. Imam, L.E. Kenyon, G. Ashby, F. Nagib, M. Mendicino, C. Zhao, A.K. Gadok, J.C. Stachowiak, Phase-Separated Liposomes Enhance the Efficiency of Macromolecular Delivery to the Cellular Cytoplasm, Cel. Mol. Bioeng. 10 (2017) 387–403. https://doi.org/10.1007/s12195-017-0489-4.
- [6] A.N. Trementozzi, Z.I. Imam, M. Mendicino, C.C. Hayden, J.C. Stachowiak, Liposome-Mediated Chemotherapeutic Delivery is Synergistically Enhanced by Ternary Lipid Compositions and Cationic Lipids, Langmuir. 35 (2019) 12532–12542. https://doi.org/10.1021/acs.langmuir.9b01965.

- [7] S.L. Veatch, S.L. Keller, Seeing spots: Complex phase behavior in simple membranes, Biochimica et Biophysica Acta (BBA) Molecular Cell Research. 1746 (2005) 172–185. https://doi.org/10.1016/j.bbamcr.2005.06.010.
- [8] D. Marsh, Cholesterol-induced fluid membrane domains: A compendium of lipid-raft ternary phase diagrams, Biochimica et Biophysica Acta (BBA) Biomembranes. 1788 (2009) 2114–2123. https://doi.org/10.1016/j.bbamem.2009.08.004.
- [9] S.L. Veatch, S.L. Keller, Miscibility Phase Diagrams of Giant Vesicles Containing Sphingomyelin, Phys. Rev. Lett. 94 (2005) 148101. https://doi.org/10.1103/PhysRevLett.94.148101.
- [10] J. Nam, T.K. Vanderlick, P.A. Beales, Formation and dissolution of phospholipid domains with varying textures in hybrid lipo-polymersomes, Soft Matter. 8 (2012) 7982–7988. https://doi.org/10.1039/c2sm25646k.
- [11] S. Winzen, M. Bernhardt, D. Schaeffel, A. Koch, M. Kappl, K. Koynov, K. Landfester, A. Kroeger, Submicron hybrid vesicles consisting of polymer lipid and polymer cholesterol blends, Soft Matter. 9 (2013) 5883–5890. https://doi.org/10.1039/C3SM50733E.
- [12] B.R. Lentz, Y. Barenholz, T.E. Thompson, Fluorescence depolarization studies of phase transitions and fluidity in phospholipid bilayers. 2. Two-component phosphatidylcholine liposomes, Biochemistry. 15 (1976) 4529–4537. https://doi.org/10.1021/bi00665a030.
- [13] T. Parasassi, G. De Stasio, G. Ravagnan, R.M. Rusch, E. Gratton, Quantitation of lipid phases in phospholipid vesicles by the generalized polarization of Laurdan fluorescence, Biophysical Journal. 60 (1991) 179–189. https://doi.org/10.1016/S0006-3495(91)82041-0.
- [14] W.F. Zeno, S. Hilt, K.K. Aravagiri, S.H. Risbud, J.C. Voss, A.N. Parikh, M.L. Longo, Analysis of Lipid Phase Behavior and Protein Conformational Changes in Nanolipoprotein Particles upon Entrapment in Sol-Gel-Derived Silica, Langmuir. 30 (2014) 9780–9788. https://doi.org/10.1021/la5025058.
- [15] K. Suga, H. Umakoshi, Detection of Nanosized Ordered Domains in DOPC/DPPC and DOPC/Ch Binary Lipid Mixture Systems of Large Unilamellar Vesicles Using a TEMPO Quenching Method, Langmuir. 29 (2013) 4830–4838. https://doi.org/10.1021/la304768f.
- [16] N. Hamada, S. Gakhar, M.L. Longo, Hybrid lipid/block copolymer vesicles display broad phase coexistence region, Biochimica et Biophysica Acta (BBA) Biomembranes. 1863 (2021) 183552. https://doi.org/10.1016/j.bbamem.2021.183552.
- [17] K. Flandez, S. Bonardd, M. Soto-Arriaza, Physicochemical properties of L-alpha dipalmitoyl phosphatidylcholine large unilamellar vesicles: Effect of hydrophobic block (PLA/PCL) of amphipathic diblock copolymers, Chemistry and Physics of Lipids. 230 (2020) 104927. https://doi.org/10.1016/j.chemphyslip.2020.104927.
- [18] N. Puff, G. Staneva, M.I. Angelova, M. Seigneuret, Improved Characterization of Raft-Mimicking Phase-Separation Phenomena in Lipid Bilayers Using Laurdan Fluorescence with Log-Normal Multipeak Analysis, Langmuir. 36 (2020) 4347–4356. https://doi.org/10.1021/acs.langmuir.0c00412.
- [19] N. Watanabe, Y. Goto, K. Suga, T.K.M. Nyholm, J.P. Slotte, H. Umakoshi, Solvatochromic Modeling of Laurdan for Multiple Polarity Analysis of Dihydrosphingomyelin Bilayer, Biophysical Journal. 116 (2019) 874–883. https://doi.org/10.1016/j.bpj.2019.01.030.
- [20] M. Bacalum, B. Zorilă, M. Radu, Fluorescence spectra decomposition by asymmetric functions: Laurdan spectrum revisited, Anal Biochem. 440 (2013) 123–129. https://doi.org/10.1016/j.ab.2013.05.031.

- [21] J.C.-M. Lee, M. Santore, F.S. Bates, D.E. Discher, From Membranes to Melts, Rouse to Reptation: Diffusion in Polymersome versus Lipid Bilayers, Macromolecules. 35 (2002) 323–326. https://doi.org/10.1021/ma0112063.
- [22] J. Mooney, P. Kambhampati, Get the Basics Right: Jacobian Conversion of Wavelength and Energy Scales for Quantitative Analysis of Emission Spectra, J. Phys. Chem. Lett. 4 (2013) 3316–3318. https://doi.org/10.1021/jz401508t.
- [23] A.D. Lúcio, C.C. Vequi-Suplicy, R.M. Fernandez, M.T. Lamy, Laurdan Spectrum Decomposition as a Tool for the Analysis of Surface Bilayer Structure and Polarity: a Study with DMPG, Peptides and Cholesterol, J Fluoresc. 20 (2010) 473–482. https://doi.org/10.1007/s10895-009-0569-5.
- [24] B. Kubsch, T. Robinson, R. Lipowsky, R. Dimova, Solution Asymmetry and Salt Expand Fluid-Fluid Coexistence Regions of Charged Membranes, Biophysical Journal. 110 (2016) 2581–2584. https://doi.org/10.1016/j.bpj.2016.05.028.
- [25] N. Watanabe, K. Suga, J.P. Slotte, T.K.M. Nyholm, H. Umakoshi, Lipid-Surrounding Water Molecules Probed by Time-Resolved Emission Spectra of Laurdan, Langmuir. 35 (2019) 6762–6770. https://doi.org/10.1021/acs.langmuir.9b00303.
- [26] R.B.M. Koehorst, R.B. Spruijt, M.A. Hemminga, Site-Directed Fluorescence Labeling of a Membrane Protein with BADAN: Probing Protein Topology and Local Environment, Biophysical Journal. 94 (2008) 3945–3955. https://doi.org/10.1529/biophysj.107.125807.
- [27] C.A. Stanich, A.R. Honerkamp-Smith, G.G. Putzel, C.S. Warth, A.K. Lamprecht, P. Mandal, E. Mann, T.-A.D. Hua, S.L. Keller, Coarsening Dynamics of Domains in Lipid Membranes, Biophysical Journal. 105 (2013) 444–454. https://doi.org/10.1016/j.bpj.2013.06.013.
- [28] T.P.T. Dao, F. Fernandes, E. Ibarboure, K. Ferji, M. Prieto, O. Sandre, J.-F. Le Meins, Modulation of phase separation at the micron scale and nanoscale in giant polymer/lipid hybrid unilamellar vesicles (GHUVs), Soft Matter. 13 (2017) 627–637. https://doi.org/10.1039/C6SM01625A.
- [29] D.J. Estes, M. Mayer, Giant liposomes in physiological buffer using electroformation in a flow chamber, Biochimica et Biophysica Acta (BBA) Biomembranes. 1712 (2005) 152–160. https://doi.org/10.1016/j.bbamem.2005.03.012.
- [30] A. Li, J. Pazzi, M. Xu, A.B. Subramaniam, Cellulose Abetted Assembly and Temporally Decoupled Loading of Cargo into Vesicles Synthesized from Functionally Diverse Lamellar Phase Forming Amphiphiles, Biomacromolecules. 19 (2018) 849–859. https://doi.org/10.1021/acs.biomac.7b01645.
- [31] J. Pazzi, A.B. Subramaniam, Nanoscale Curvature Promotes High Yield Spontaneous Formation of Cell-Mimetic Giant Vesicles on Nanocellulose Paper, ACS Appl. Mater. Interfaces. 12 (2020) 56549–56561. https://doi.org/10.1021/acsami.0c14485.
- [32] S.L. Veatch, S.L. Keller, Separation of Liquid Phases in Giant Vesicles of Ternary Mixtures of Phospholipids and Cholesterol, Biophysical Journal. 85 (2003) 3074–3083. https://doi.org/10.1016/S0006-3495(03)74726-2.

# **Supplementary Material**

Characterization of phase separation phenomena in hybrid lipid/block copolymer/cholesterol bilayers using laurdan fluorescence with log-normal multipeak analysis

Naomi Hamada<sup>a</sup> and Marjorie L. Longo\*<sup>a</sup>

<sup>a</sup> Department of Chemical Engineering, University of California Davis, Davis, California 95616, United States

\*Email: mllongo@ucdavis.edu

## **Table of contents:**

# S1. Supplementary Figures

Figure S1

Figure S2

Figure S3

Figure S4

Figure S5

# **S2. Supplementary Tables**

Table S1

Table S2

#### S1. Supplementary Figures

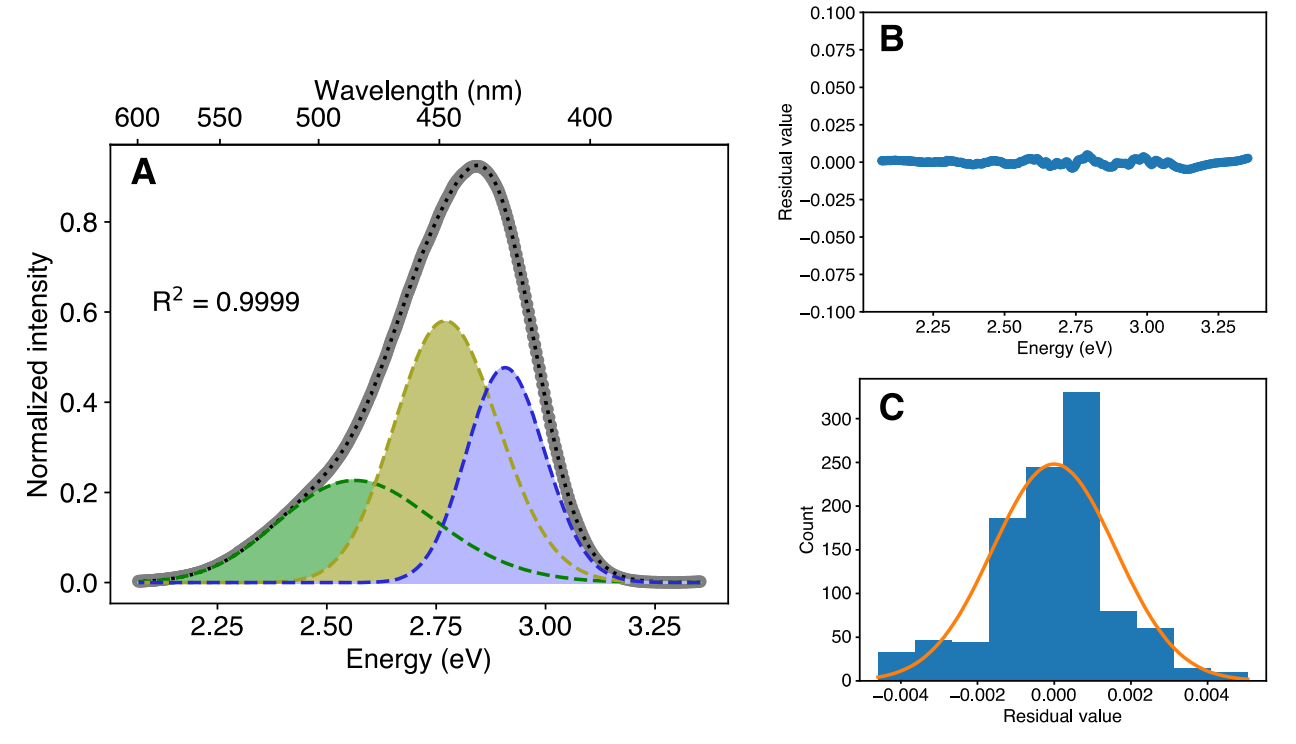


Figure S1. A. Example of a three-peak fit to the emission spectrum of laurdan in 30-40-30 mol% POPC-egg SM-cholesterol LUVs at 20 °C. Green peak is low-eV, yellow peak is mid-eV, purple peak is high-eV. B. Residual values for the peak fit. C. Residual histogram and corresponding distribution (orange overlay). Relatively small residual values and Gaussian residual distribution suggest a reasonably accurate fit.

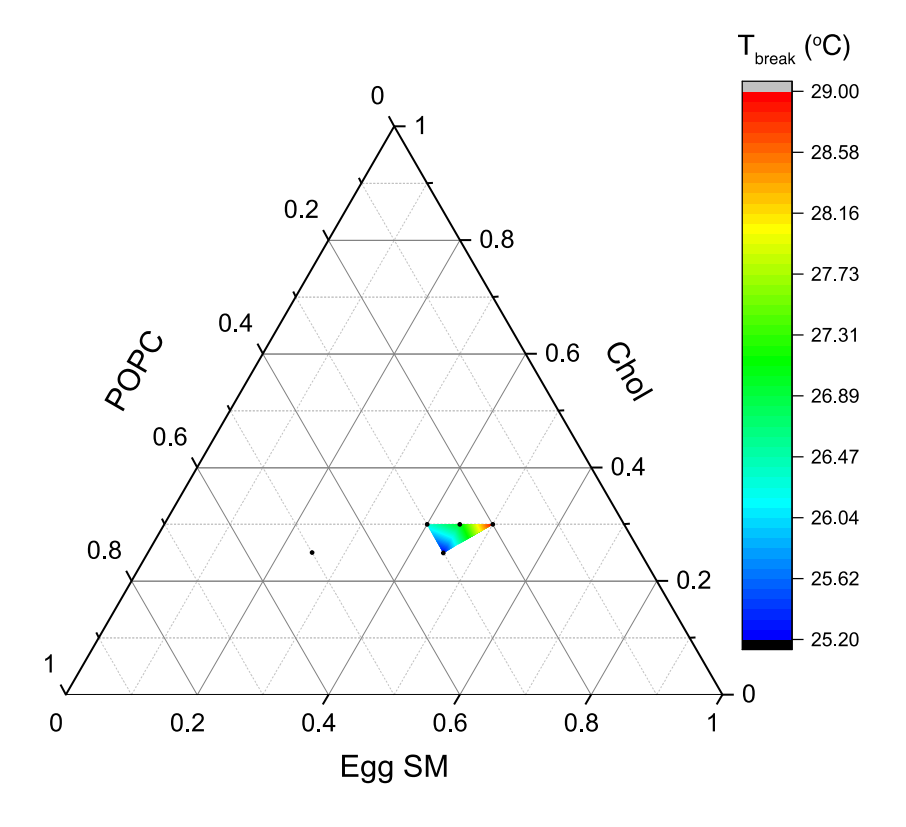


Figure S2. Heat map of  $T_{break}$  values indicated by three-peak decomposition of laurdan emission spectra in POPC-egg SM-cholesterol LUVs. For the single point plotted outside the edges of the heat map, only a single phase was observed for GUVs at the lowest accessible temperature (~13 °C).

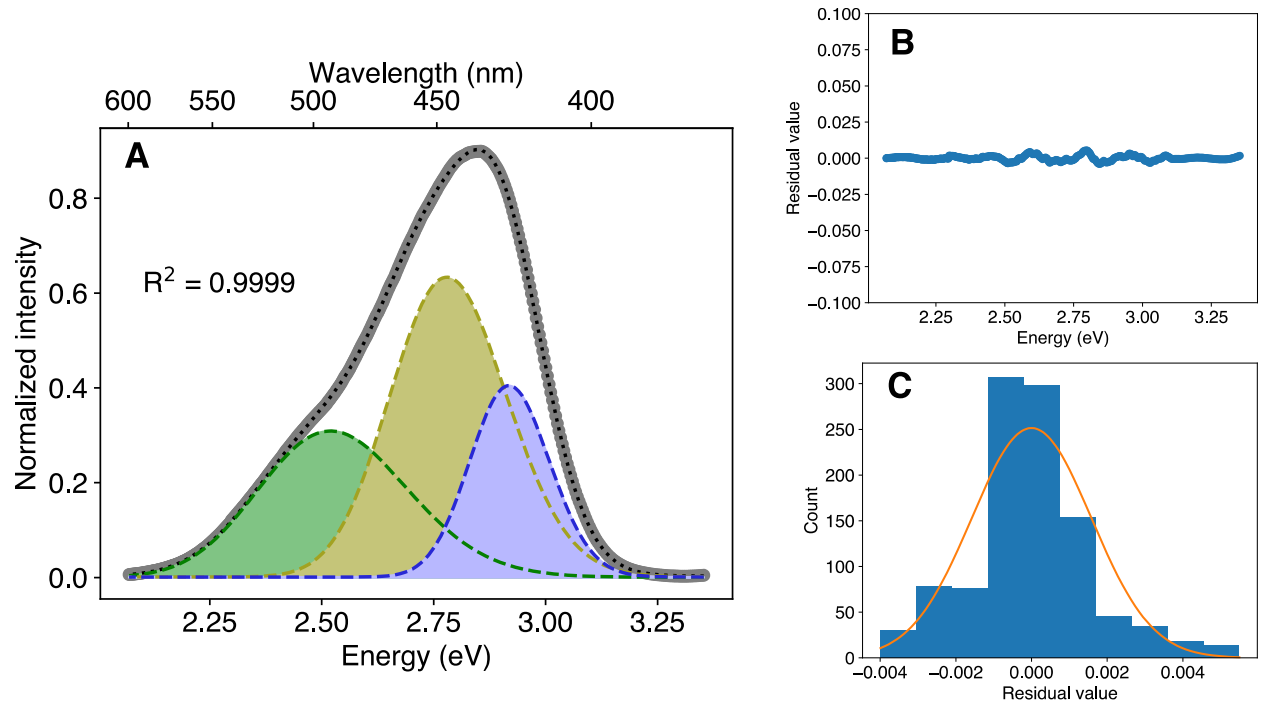


Figure S3. A. Three peak fit of laurdan emission spectrum in 30-40-30 mol% PBdPEO-egg SM-chol LUVs at 20 °C. Green peak is low-eV, yellow peak is mid-eV, purple peak is high-eV. B. Residual values as a function of position. C. Residual histogram and corresponding distribution (orange overlay). Relatively small residual values and Gaussian residual distribution suggest a reasonably accurate fit.

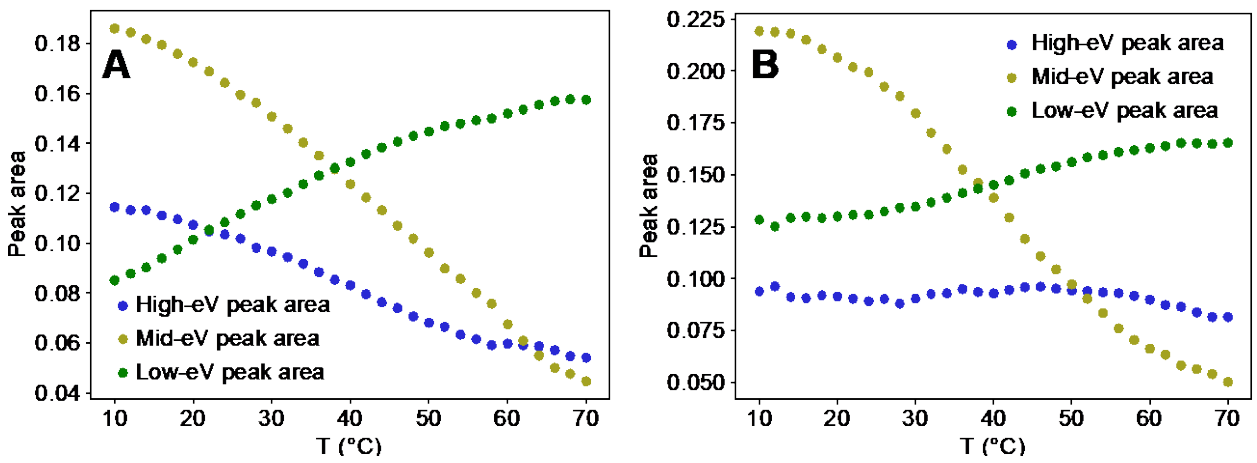


Figure S4. A. Temperature dependence of the areas of peaks returned from decomposition of laurdan emission spectra in 30-40-30 mol% POPC-egg SM-cholesterol LUVs. Steady decrease of the area of the high-eV peak with increasing temperature is evident. B. Peak areas returned from laurdan emission spectra decomposition for 30-40-30 mol% PBdPEO-egg SM-cholesterol LUVs. The area of the high-eV peak remains relatively constant with temperature, unlike the trend observed for the lipid-only vesicles.

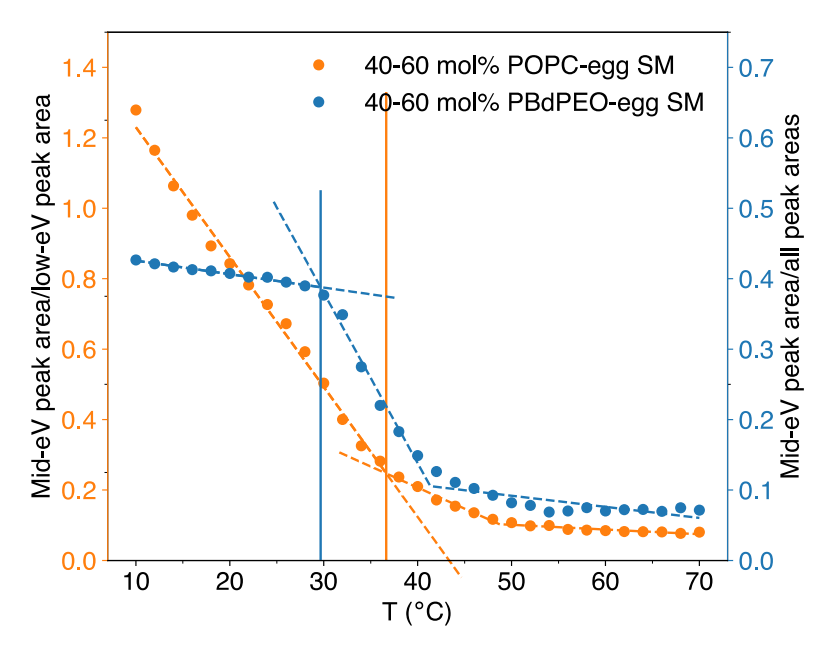


Figure S5. Comparison of three-peak analysis of laurdan emission spectra for cholesterol-free vesicles composed of either 40-60 mol% POPC-egg SM or 40-60 mol% PBdPEO-egg SM. The ratios of the areas of the mid-eV and low-eV peaks (left y-axis) are plotted for POPC-egg SM vesicles. For PBdPEO-egg SM vesicles, the areas of the mid-eV peaks are compared to the sum of the areas of all peaks (right y-axis), based on the finding that this yielded a  $T_{break}$  more consistent with GUV  $T_m$  results for hybrid vesicles. Dashed lines indicate the piecewise linear function used to evaluate  $T_{break}$ .

## S2. Supplementary Tables

Table S1. Comparison of the miscibility temperatures observed in GUVs ( $T_m$ ) and indicated by laurdan in POPC-egg SM-cholesterol LUVs ( $T_{break}$ ).  $T_{break}$  was determined from the ratios of the areas of the mid-eV and low-eV peaks resulting from decomposition of laurdan emission spectra into three peaks. Experimental uncertainty in  $T_m$  was determined to be roughly a range of 1.5 °C, based on repeated experiments with selected compositions of GUV. Uncertainty values in  $T_{break}$  are obtained from the standard deviation error in the piecewise linear fit to the peak area ratio values.

POPC-egg SM-chol (mol%)	T <sub>m</sub> (°C)	T <sub>break</sub> (°C)
30-40-30	28.0±1.5	26.3±0.9
25-45-30	32.0±1.5	27.0±1.2
30-45-25	26.5±1.5	25.2±0.8
20-50-30	30.5±1.5	29.0±0.7

Table S2. Comparison of the miscibility temperatures observed in GUVs ( $T_m$ ) and indicated by laurdan in PBdPEO-egg SM-cholesterol LUVs ( $T_{break}$ ).  $T_{break}$  was determined from the ratios of the areas of the mid-eV and low-eV peaks resulting from decomposition of laurdan emission spectra into three peaks;  $T_{break}$  was also refitted by calculating the ratio of the area of the mid-eV peak to the total area of all three peaks. Asterisk (\*) indicates  $T_m$  was determined upon heating rather than cooling. Experimental uncertainty in  $T_m$  was determined to be roughly a range of 1.5 °C, based on repeated experiments with selected compositions of GUV. Uncertainty values in  $T_{break}$  are obtained from the standard deviation error in the piecewise linear fit to the peak area ratio values.

PBdPEO-egg SM-chol (mol%)	T <sub>m</sub> (°C)	T <sub>break</sub> (°C)	T <sub>break</sub> , refitted (°C)
30-40-30	29.5±1.5	24.3±0.8	27.2±0.4
25-45-30	31.5±1.5	23.0±0.5	28.8+0.9
30-45-25	29.5±1.5	24.8±0.5	29.1±1.0
20-50-30	29.0±1.5	29.4±0.8	30.1±0.9
35-25-40	27.0±1.5	26.0±0.2	25.9±0.2
20-30-50	None observed.	-	-
50-25-25	30-32*	27.2±0.1	27.2±0.1

# **Supplementary Material**

Characterization of phase separation phenomena in hybrid lipid/block copolymer/cholesterol bilayers using laurdan fluorescence with log-normal multipeak analysis

Naomi Hamada<sup>a</sup> and Marjorie L. Longo\*<sup>a</sup>

<sup>a</sup> Department of Chemical Engineering, University of California Davis, Davis, California 95616, United States

\*Email: mllongo@ucdavis.edu

## **Table of contents:**

# S1. Supplementary Figures

Figure S1

Figure S2

Figure S3

Figure S4

Figure S5

# **S2. Supplementary Tables**

Table S1

Table S2

## S1. Supplementary Figures

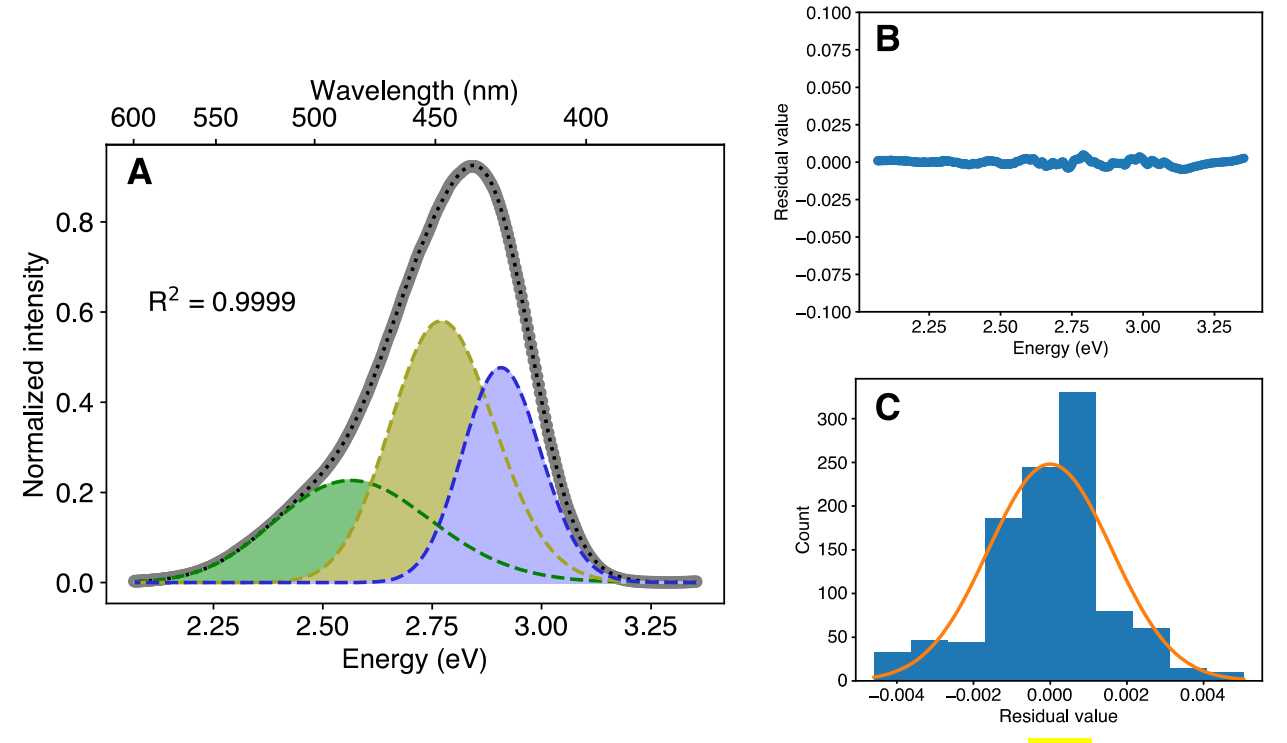


Figure S1. A. Example of a three-peak fit to the emission spectrum of laurdan in 30-40-30 mol% POPC-egg SM-cholesterol LUVs at 20 °C. Green peak is low-eV, yellow peak is mid-eV, purple peak is high-eV. B. Residual values for the peak fit. C. Residual histogram and corresponding distribution (orange overlay). Relatively small residual values and Gaussian residual distribution suggest a reasonably accurate fit.

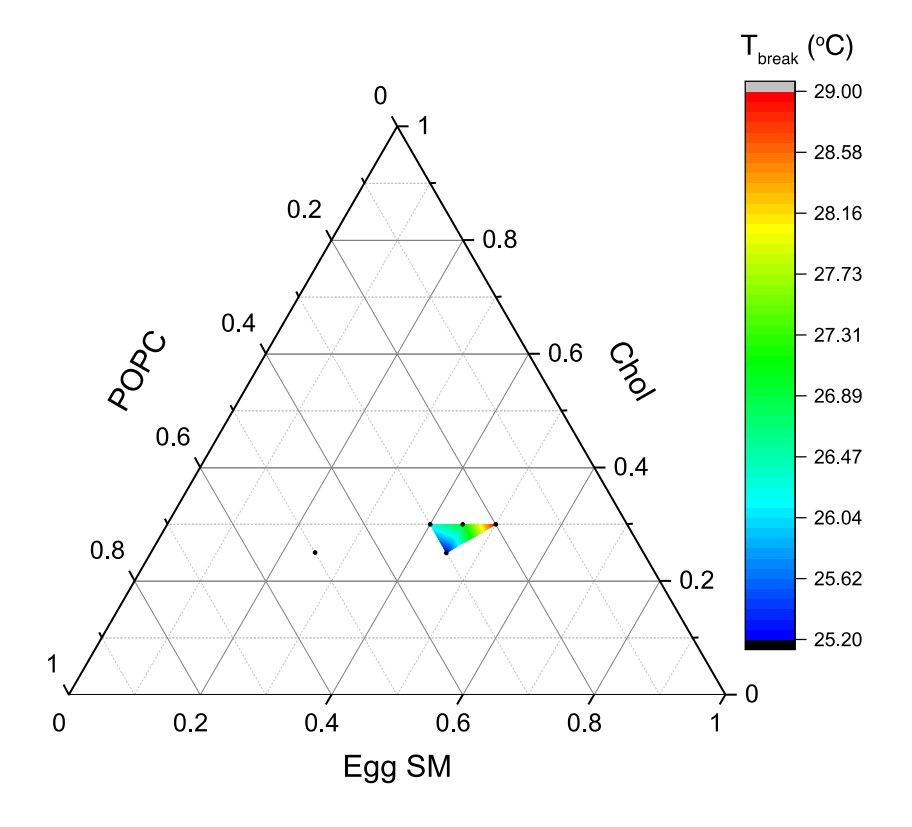


Figure S2. Heat map of  $T_{break}$  values indicated by three-peak decomposition of laurdan emission spectra in POPC-egg SM-cholesterol LUVs. For the single point plotted outside the edges of the heat map, only a single phase was observed for GUVs at the lowest accessible temperature (~13 °C).

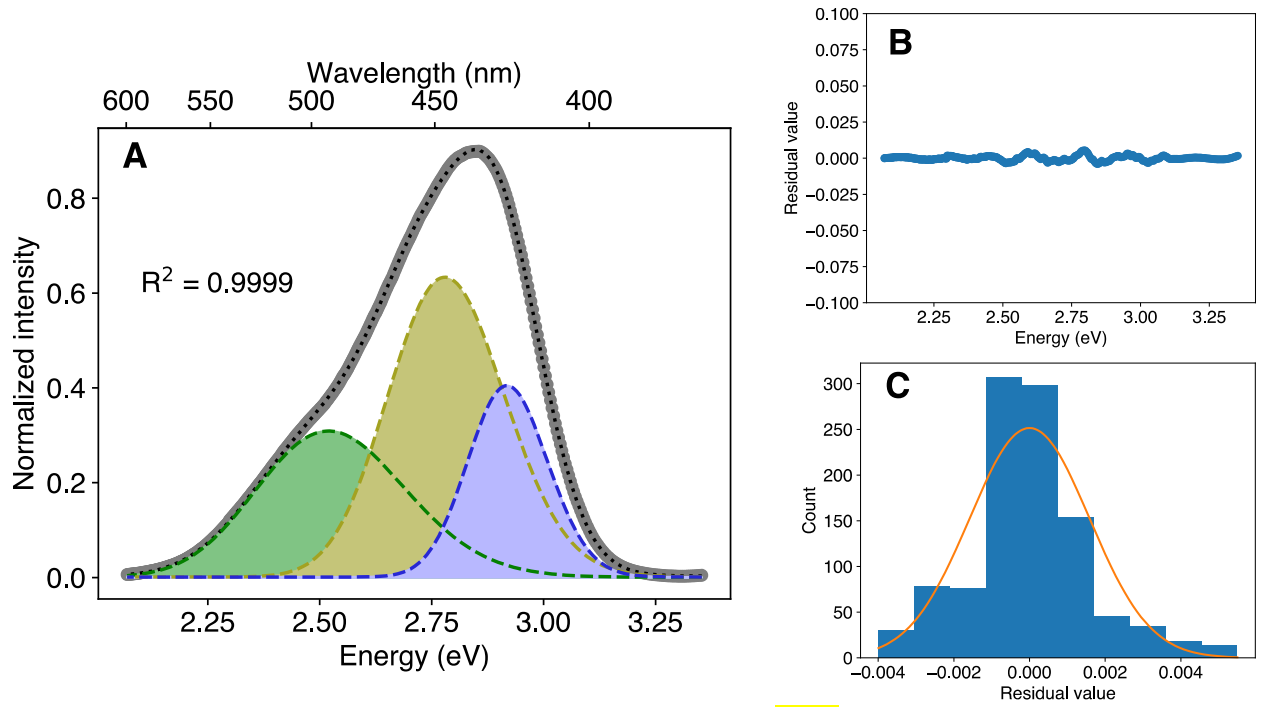


Figure S3. A. Three peak fit of laurdan emission spectrum in 30-40-30 mol% PBdPEO-egg SM-chol LUVs at 20 °C. Green peak is low-eV, yellow peak is mid-eV, purple peak is high-eV. B. Residual values as a function of position. C. Residual histogram and corresponding distribution (orange overlay). Relatively small residual values and Gaussian residual distribution suggest a reasonably accurate fit.

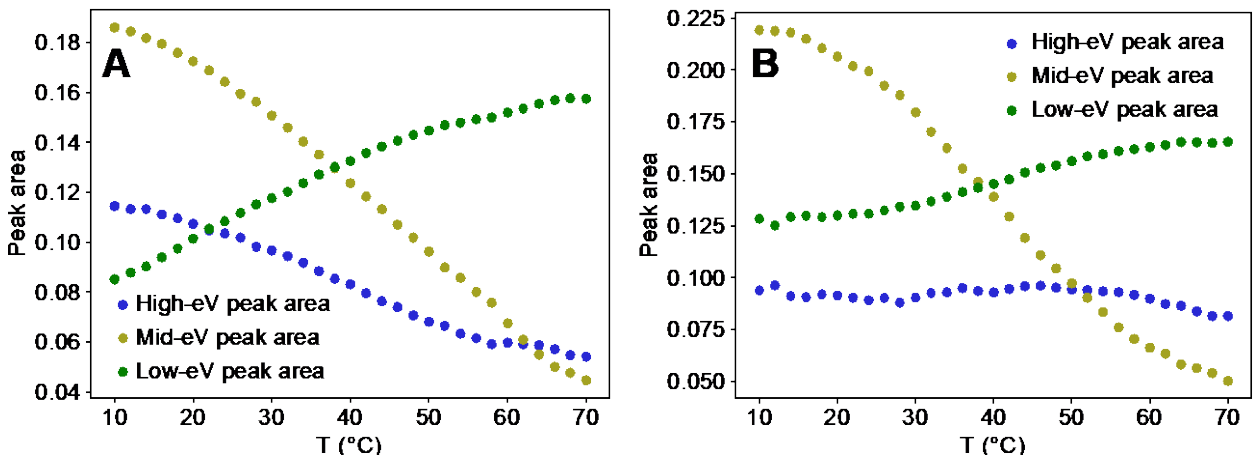


Figure S4. A. Temperature dependence of the areas of peaks returned from decomposition of laurdan emission spectra in 30-40-30 mol% POPC-egg SM-cholesterol LUVs. Steady decrease of the area of the high-eV peak with increasing temperature is evident. B. Peak areas returned from laurdan emission spectra decomposition for 30-40-30 mol% PBdPEO-egg SM-cholesterol LUVs. The area of the high-eV peak remains relatively constant with temperature, unlike the trend observed for the lipid-only vesicles.

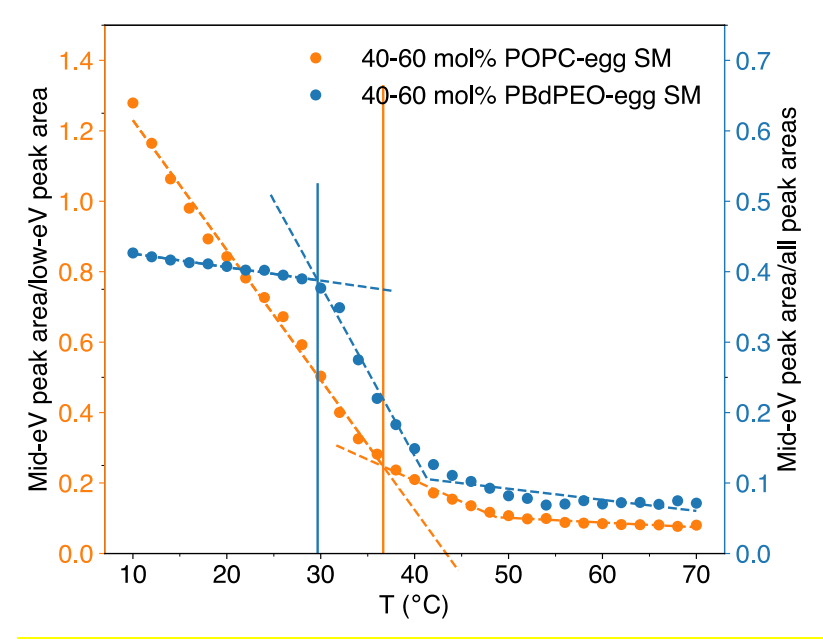


Figure S5. Comparison of three-peak analysis of laurdan emission spectra for cholesterol-free vesicles composed of either 40-60 mol% POPC-egg SM or 40-60 mol% PBdPEO-egg SM. The ratios of the areas of the mid-eV and low-eV peaks (left y-axis) are plotted for POPC-egg SM vesicles. For PBdPEO-egg SM vesicles, the areas of the mid-eV peaks are compared to the sum of the areas of all peaks (right y-axis), based on the finding that this yielded a T<sub>break</sub> more consistent with GUV T<sub>m</sub> results for hybrid vesicles. Dashed lines indicate the piecewise linear function used to evaluate T<sub>break</sub>.

### S2. Supplementary Tables

Table S1. Comparison of the miscibility temperatures observed in GUVs ( $T_m$ ) and indicated by laurdan in POPC-egg SM-cholesterol LUVs ( $T_{break}$ ).  $T_{break}$  was determined from the ratios of the areas of the mid-eV and low-eV peaks resulting from decomposition of laurdan emission spectra into three peaks. Experimental uncertainty in  $T_m$  was determined to be roughly a range of 1.5 °C, based on repeated experiments with selected compositions of GUV. Uncertainty values in  $T_{break}$  are obtained from the standard deviation error in the piecewise linear fit to the peak area ratio values.

POPC-egg SM-chol (mol%)	T <sub>m</sub> (°C)	T <sub>break</sub> (°C)
30-40-30	28 <mark>.0±1.5</mark>	26.3±0.9
25-45-30	32 <mark>.0±1.5</mark>	27.0±1.2
30-45-25	26.5 <mark>±1.5</mark>	25.2±0.8
20-50-30	30.5±1.5	29.0 <del>±0.7</del>

Table S2. Comparison of the miscibility temperatures observed in GUVs (T<sub>m</sub>) and indicated by laurdan in PBdPEO-egg SM-cholesterol LUVs (T<sub>break</sub>). T<sub>break</sub> was determined from the ratios of the areas of the mid-eV and low-eV peaks resulting from decomposition of laurdan emission spectra into three peaks; T<sub>break</sub> was also refitted by calculating the ratio of the area of the mid-eV peak to the total area of all three peaks. Asterisk (\*) indicates T<sub>m</sub> was determined upon heating rather than cooling. Experimental uncertainty in T<sub>m</sub> was determined to be roughly a range of 1.5 °C, based on repeated experiments with selected compositions of GUV. Uncertainty values in T<sub>break</sub> are obtained from the standard deviation error in the piecewise linear fit to the peak area ratio values.

PBdPEO-egg SM-chol (mol%)	T <sub>m</sub> (°C)	T <sub>break</sub> (°C)	T <sub>break</sub> , refitted (°C)
30-40-30	29.5 <mark>±1.5</mark>	24.3 <mark>±0.8</mark>	27.2 <mark>±0.4</mark>
25-45-30	31.5 <mark>±1.5</mark>	23.0 <del>±0.5</del>	28.8 <mark>+0.9</mark>
30-45-25	29.5 <mark>±1.5</mark>	24.8±0.5	29.1 <mark>±1.0</mark>
20-50-30	29 <mark>.0±1.5</mark>	29.4 <mark>±0.8</mark>	30.1 <del>±0.9</del>
35-25-40	27 <mark>.0±1.5</mark>	26 <mark>.0±0.2</mark>	25.9 <mark>±0.2</mark>
20-30-50	None observed.	-	-
50-25-25	30-32*	27.2 <mark>±0.1</mark>	27.2 <mark>±0.1</mark>

Declaration of Interest Statement

**Declaration of interests** 

oxtimes The authors declare that they have no known competing financial interests or personal relationships that could have appeared to influence the work reported in this paper.	
□The authors declare the following financial interests/personal relationships which may be considered as potential competing interests:	
	_